

# Genesis and Implications of the Composition and Sedimentary Structure of Fine-Grained Carbonate Rocks in the Shulu Sag

Xiangxin Kong<sup>1,2</sup>, Zaixing Jiang<sup>1,2\*</sup>, Chao Han<sup>3</sup>, Lijing Zheng<sup>4</sup>, Yiming Zhang<sup>5</sup>,  
Ruifeng Zhang<sup>5</sup>, Jianzhang Tian<sup>5</sup>



1. School of Energy Resources, China University of Geosciences, Beijing 100083, China

2. Institute of Earth Sciences, China University of Geosciences, Beijing 100083, China

3. College of Earth Science and Engineering, Shandong University of Science and Technology, Qingdao 266590, China

4. Institute of Geology and Geophysics, Chinese Academy of Sciences, Beijing 100029, China

5. PetroChina Huabei Oilfield Company, Renqiu 062552, China

 Xiangxin Kong: <http://orcid.org/0000-0003-1778-4246>;  Zaixing Jiang: <http://orcid.org/0000-0002-2373-5574>

**ABSTRACT:** Fine-grained carbonate rocks, which extensively occur in the Eocene strata in the Shulu sag, Bohai Bay Basin, North China, represent an unconventional, fine-grained carbonate reservoir. However, previous studies have ignored the complexity of the lithofacies components and their formation mechanisms. Fine-grained carbonate rocks are typical reservoirs in which hydrocarbons form and gather. A better understanding of the nature of these rocks is extremely important for evaluating the quality of unconventional, fine-grained carbonate reservoirs. Various lithofacies components were discriminated in this study with a combination of petrographic observations and carbon isotope analyses. These fine-grained carbonate rocks comprise terrigenous, biogenic and diagenetic materials. Terrigenous input and biologically induced precipitation are the main sources of the materials in the lake. Five lithofacies were identified based on the observations of sedimentary features (core and thin section) and mineralogical data: (1) varve-like laminated calcilutite, (2) graded laminated calcilutite, (3) interlaminated calcisiltite-calcilutite, (4) massive calcilutite, and (5) massive calcisiltite-calcarenite. Their origins were recorded by various lithofacies components, which are controlled by the interactions of physical, chemical and biological processes. This study indicated that the lithology of the bedrocks was the key factor controlling carbonate accumulation. The tectonics and climate can influence the weathering and types of lithofacies. Primary productivity controlled the precipitation of the endogenic calcite. These factors jointly determined the abundant fine-grained carbonate rocks that have accumulated in the Shulu sag.

**KEY WORDS:** fine-grained carbonate rocks, terrigenous materials, biologically induced precipitation, varve, carbon isotope, massive calcilutite.

## 0 INTRODUCTION

Fine-grained carbonate rocks, which widely occur in the Eocene strata in the Bohai Bay Basin, North China, represent a special lacustrine component and act as the key source rocks for oil and gas fields in continental basins (Huang et al., 2015; Pu et al., 2011; Wang et al., 2010; Jin et al., 2002; Chang, 1991). Recent success in the exploration and development of hydrocarbons from unconventional, fine-grained reservoirs has inspired research on self-sourced systems (Jarvie, 2012a, b). A better understanding of fine-grained carbonate rocks is the basis for the production of lacustrine carbonate-rich unconventional reservoirs.

The Shulu sag is located in the south-western corner of the Jizhong (central Hebei) depression in the Bohai Bay Basin (Jiang et al., 2007). The lake basin is characterized by abundant carbonate sediments in the lower member of the Shahejie 3 Formation. Compared with palustrine and shallow lake carbonates (Freytet and Verrecchia, 2002; Platt and Wright, 1991), the fine-grained carbonate rocks in the Shulu sag mainly occur in deep lake. These rocks predominantly comprise micritic calcite. However, a large number of thick-layer carbonate rudstones have accumulated on the western slope in shallow water. Previous research has considered the carbonate deposition (both micritic calcite and carbonate rudstone) to be related to mechanical transport from the Early Paleozoic marine carbonate bedrocks in the western uplift (Qiu et al., 2010). However, researchers have become aware of the complexity of the origin of fine-grained carbonate rocks with the development of oil production in the oil-bearing pools. Although productive studies have been conducted on carbonate rudstones (Jiang et al., 2007)

\*Corresponding author: [jiangzx@cugb.edu.cn](mailto:jiangzx@cugb.edu.cn)

© China University of Geosciences and Springer-Verlag GmbH Germany 2017

Manuscript received March 10, 2016.

Manuscript accepted November 17, 2016.

and organic matter-rich, unconventional, fine-grained carbonate reservoirs (Zhao et al., 2014; Jiang and Li, 2013), the different sources of carbonate materials and the origin of sedimentary structures (e.g., lamination and massive nature) have been ignored during the past decade.

Widespread carbonate sediments, both modern and ancient, accumulate in lakes (Hargrave et al., 2014; Platt, 1989; Dean, 1981). Most of these sediments accumulate in the form of mud-sized matter (Gierlowski-Kordesch, 2010). The compositions of lacustrine, fine-grained carbonate rocks indicate the interactions of physical, chemical, and biological processes, as with other mudstones, including extrabasinal and intrabasinal grains (Milliken, 2014). The components of fine-grained rocks can influence the evolution of the bulk rock's attributes (Macquaker et al., 2007). Understanding the complexity of compositional variation in fine-grained assemblages is still a challenge. Lamination and massive features are very common in lacustrine fine-grained carbonate rocks (Hilfinger et al., 2001; Soreghan, 1998); however, their origins are complex and varied (Dean et al., 2006; Tucker and Wright, 1990). The general terminology of "laminated, fine-grained carbonate rocks" includes all of the rocks in the study area with a single-layer thickness less than 1 cm; however, the term ignores the differences in their microscopic geometric features and components. The traditional view considers lacustrine massive mudstones or structure-less fine-grained carbonate rocks to be formed by bioturbation in shallow water (Anadón et al., 2000; Ramos-Guerrero et al., 2000). However, the thick massive calcilitites in the Shulu sag are analogous to deep water uniffites or homogeneous mud (Behrens, 1984; Stanley, 1981). These sedimentary structures are key characteristics that reflect the sediment accumulation rate and lake water column energy (Lazar et al., 2015); therefore, further study on the fine-grained carbonate rocks in the Shulu sag is extremely important for understanding deposition processes and evaluating the quality of unconventional, fine-grained carbonate reservoirs.

The major objectives of this paper are as follows: (1) to discriminate grains of different origins and contrast the various sources of components in different lithofacies; and (2) to describe different lithofacies based on their composition and sedimentary structural characteristics and explain the origin of the fine-grained carbonate rocks in the study area.

These studies can provide useful evidence for understanding the mineralogical and textural heterogeneity of the fine-grained carbonates in the Shulu sag.

## 1 GEOLOGIC SETTING

The Shulu sag, which is located in the south-western corner of the Jizhong depression in the Bohai Bay Basin (Fig. 1), is an elongate half-graben basin that is oriented north-east/south-west (Figs. 2a, 2b). The sag covers 300 km<sup>2</sup> and was formed through the downthrow of the hanging wall of the Xinhe fault, which is located along the south-eastern Paleogene boundary (Jiang et al., 2007). The sediment fills within the basin increasingly overlap upward upon the western slope and link with the Ningjin uplift (Fig. 2d). The WE to WNE-ESE trending antecedent faults (e.g., Hengshui fault, Taijiazhuang fault and Jingqiu fault) divided the basin into three segments: the northern, middle and southern

segments (Fig. 2b) (Zhao et al., 2014; Jiang et al., 2007). The western slope and slope break in the middle segment are the focus of this study.

The basement of the half-graben comprises Archean-Paleoproterozoic metamorphic rocks and Meso-Neoproterozoic through Paleozoic sedimentary strata (Jiang et al., 2007). Cambro-Ordovician marine carbonate strata, including limestones and dolomites, are gradually exposed westwards, forming the predominant provenance area (Fig. 2d). The underlying Paleozoic strata are directly overlain by Paleogene lacustrine basin fills. The overlying strata from top to bottom include the Pingyuan, Minghuazhen, Guantao, Dongying and Shahejie formations (Fig. 2c). Three members are present in the Shahejie Formation: No. 1 (Es<sub>1</sub>), No. 2 (Es<sub>2</sub>), and No. 3 (Es<sub>3</sub>) (Zhao et al., 2014; Jiang et al., 2007). Shahejie 3 can be spilt further into three units: (1) lower clastic carbonate rudstones and fine-grained carbonate rocks; (2) middle argillaceous marlstones intercalated with shales; and (3) upper dark-grey mudstones that are interbedded with fine-grained sandstones. The lower region of Shahejie 3 is the focus of this study and can be divided into five sequences (Zheng et al., 2015).

The lake basin contained alluvial fan systems and deep lake systems during the carbonate filling (Jiang et al., 2007). The alluvial fan systems can be grouped into three facies associations: mid-proximal alluvial fan, distal alluvial fan and fan fringe (Jiang et al., 2007). The mid-proximal alluvial fan mainly includes matrix- and clast-supported carbonate rudstones, which accumulated on the mid-upper western slope. The distal alluvial fan is characterized by matrix-supported carbonate rudstones, mixed-source carbonate rudstones and calcarenites, which occur in the mid-lower western slope. The fan fringe is the transitional facies between the alluvial fan and deep lake and contains

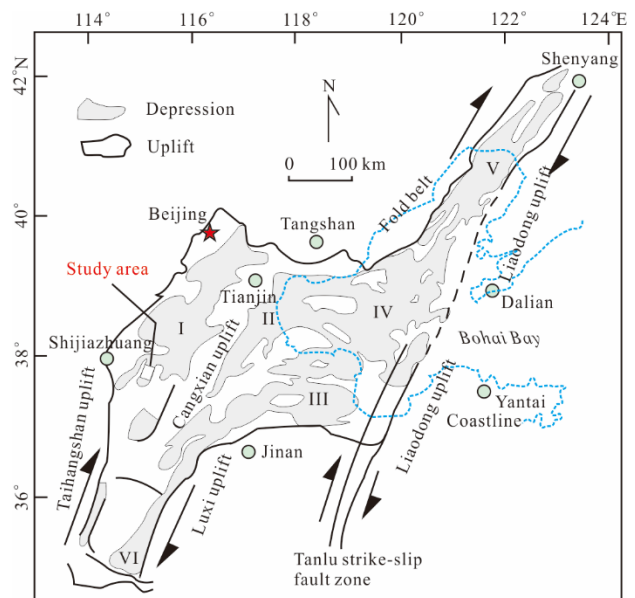


**Figure 1.** Tectonic setting of the Bohai Bay Basin (Jiang et al., 2007). The Shulu sag is located in the south-western corner of the Jizhong depression (I). Other sub-basins include the Huanghua depression (II), Jiyang depression (III), Bozhong depression (IV), Liaohe depression (V) and Dongpu depression (VI) (modified after Jiang et al., 2007).

calcsiltites and calcilutites. The profundal zone mainly comprises fine-grained carbonate rocks, including laminated and massive sediments (Zheng et al., 2015).

2 SAMPLES AND METHODS

In this study, approximately 300 m of core and cutting samples were obtained from 9 wells (Fig. 2b) in the study area (Table 1). Fine-grained carbonate rocks predominantly occur in the wells of Shutan 3 (St3), Shutan 1h (St1h), Jin 116x (J116x), Jin 85x (J85x), and Jin 97 (J97), which are close to the middle sub-sag (Fig. 2b).

Whole-rock mineralogical analyses were undertaken by the Research Institute of Petroleum Exploration and Development of the PetroChina Huabei Oilfield. A D8 DISCOVER X-Ray Diffractometer (XRD) with Cu-K $\alpha$  radiation, a voltage of 40 kV, and a current of 25 mA was used for XRD analysis. Samples were dried at a temperature of than 60 °C for 2 days and then ground to <40  $\mu$ m using an agate pestle and mortar. The sample

powders were scanned from 3° to 70° with a counting step of 0.02° and a rate of 2° per minute. Computer analyses of X-ray diffractograms, which confirmed the relationship between the mineral content and the intensity of the diffraction peak, provided semi-quantitative relative abundances (in weight percent) of the various minerals.

Total organic carbon (TOC) determination is a generally applicable method for characterizing fine-grained source rocks. The method for determining the TOC in sediments involves the combustion (oxidation) of the rock sample to convert the total organic carbon into CO<sub>2</sub> and CO at high temperatures (Charles and Simmons, 1986). Samples were grounded to <200  $\mu$ m using an agate pestle and mortar. Sample powders of less than 1 g were weighed and treated with excessive diluted hydrochloric acid (HCl). The residue samples washed with distilled water and dried in a drying oven were measured by a LECO CS-200 carbon analyser at the Research Institute of Petroleum Exploration and Development of the PetroChina Huabei Oilfield.

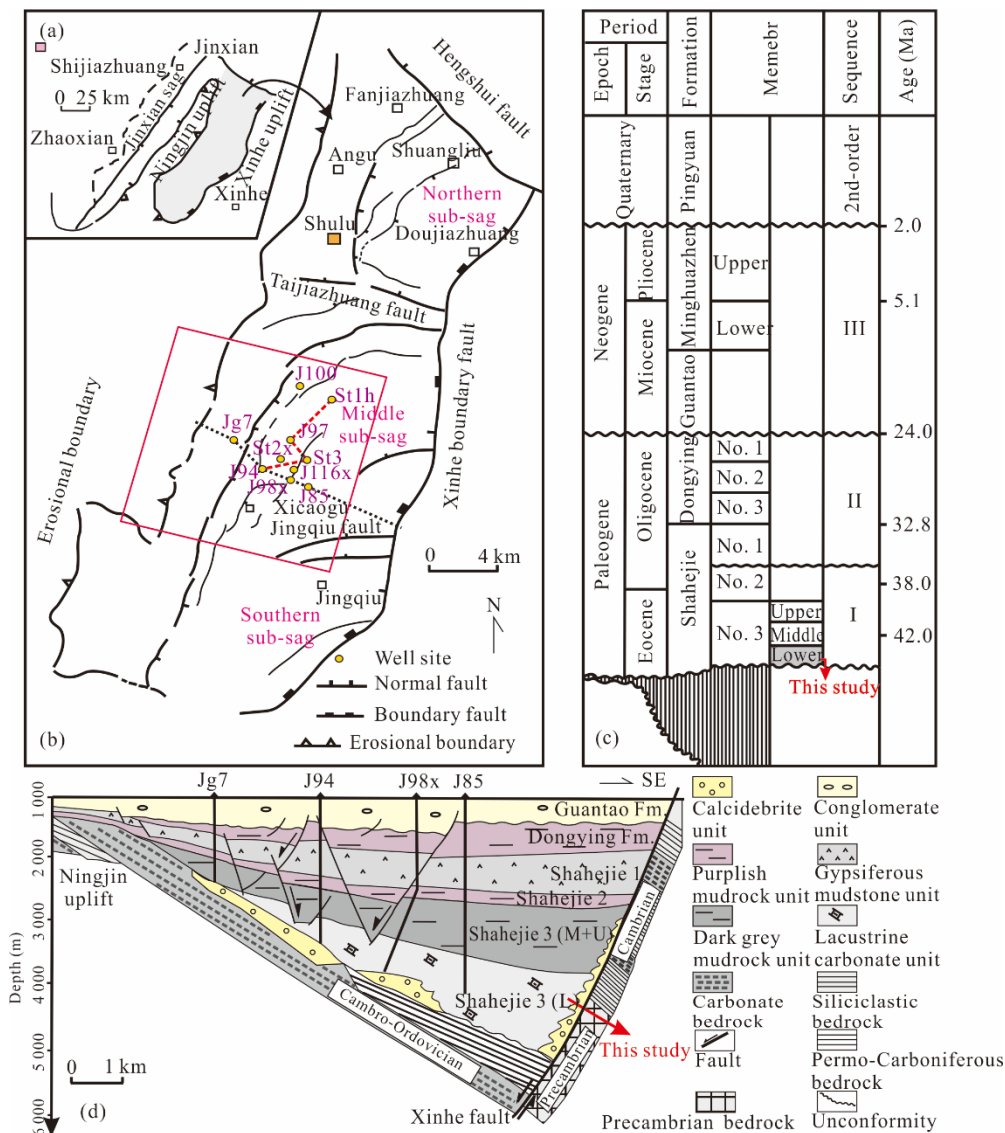


Figure 2. (a) Sketch map of Shulu sag, (b) structural map of the Shulu half-graben, which is bounded by the Hengshui fault, Xinhe fault and Ningjin uplift to the north, southeast and west, respectively (Jiang et al., 2007), (c) stratigraphic framework of the Shulu sag (modified after Zheng et al., 2015; Jiang et al., 2007), (d) transverse section across the middle segment of the Shulu sag (modified after Zhao et al., 2014).

**Table 1** Statistics of the coring wells

Number	Well	Location	Total length of core (m)	Oil daily products (t)	Production strata
1	St3	Slope break	156.26	67.32	Sequences I and II
2	St1h	Slope break	63.44	36.14	Sequence II
3	St2x	Middle slope	8.00		
4	J97	Middle slope	30.46	14.80	Sequences I–III
5	J116x	Lower slope	9.18	13.50	Sequences I–III
6	J85	Slope break	14.87		
7	J98x	Lower slope	4.45	13.45	Sequences I and II
8	J94	Upper slope	11.07		
9	J100	Upper slope	9.38		
Total			307.11		

The oil production data were derived from Zhao et al. (2015).

The carbon-stable isotopes of the whole-rock were determined by the Gas Bench II continuous flow method (Zha et al., 2010). One-hundred-milligram powder samples were weighed and placed into 12 mL containers. Then, the samples were fed into helium of 99.999% purity for air removal with a flushing time of 600 s at a flow rate of 100 mL/min and dissolved with 5 drops of phosphoric acid (100%) at 72 °C until reaction equilibrium. The mixed gases were collected, and CO<sub>2</sub> was separated from the other gases using a fused-silica tube (Poraplot Q, 25 m×0.32 mm) at 70 °C. Ultimately, the carbon isotope compositions were measured by the MAT253 mass spectrometer at the Key Laboratory of Metallogeny and Mineral Assessment, Institute of Mineral Resources, Chinese Academy of Geological Sciences. The S-4800 Field Emission Scanning Electronic Microscope (made by Hitachi, Japan) at the Center of Analysis and Testing, Beijing Normal University, and Quanta 200F Field Emission Scanning Electronic Microscope (made by FEI, Hillsboro, USA) at the Microstructure Laboratory for Energy Materials, China University of Petroleum (Beijing) were used in this study to obtain high-resolution images.

### 3 RESULTS

The systematic analyses and descriptions of each lithofacies are summarized in Table 2. The main sedimentary features of the fine-grained carbonate rocks include laminated and massive structures. These characteristics represent different transport and depositional processes. The laminations can be further divided into two types based on their geometry and shape features, e.g., varve-like laminae and silt- and mud-size graded laminae (Zolitschka et al., 2015; Lambert and Hsü, 1979a, b). The materials within fine-grained carbonate rocks were controlled by physical, chemical, and biological processes. These materials can be grouped into three types according to their origins: terrigenous, biogenic and diagenetic components (Lazar et al., 2015; Macquaker et al., 2007).

#### 3.1 Terrigenous Components

##### 3.1.1 Terrigenous calcite

Two types of calcareous macro-particles were recognized in the fine-grained carbonate rocks. The first exhibits a relatively whole monocrystalline shape with broken edges and obvious cleavage (Fig. 5a). The second displays an incomplete appearance and obscure cleavage (Fig. 5b). The latter comprises micro-grains within its body, which indicates that this type was

derived from terrigenous micritic limestone debris. These particles, whose sizes mainly range in the fine-sand to silt size, mainly accumulate in interlaminated calcisiltite-calcilutites and graded laminated calcilutites (Figs. 4d, 4e). Additionally, these particles occur in massive calcilutites as scattered components (Fig. 4f).

##### 3.1.2 Terrigenous dolomite

Compared with the larger dolostone lithoclasts in carbonate mudstones, the smaller dolomite grains, which have a relatively complete monocrystalline shape, are mainly concentrated in the 10–100 µm fraction. These grains were mainly observed in interlaminated calcisiltite-calcilutites, showing a non-orientated arrangement (Fig. 5c). They are surrounded by calcareous cement (Fig. 4e) and display obvious fracture surfaces (Fig. 5c), representing breakage from mechanical transport and collision. Only a small number of dolomite macro-particles were found in the other lithofacies.

##### 3.1.3 Clay

The shapes of the fine-grained clays are mainly platy and fibrous (Fig. 5d). One of these types is distributed in the varve-like laminated calcilutites, while the other surrounds the particles in massive calcilutites or interlaminated calcisiltite-calcilutites. Additionally, a certain amount of clay occurred in massive calcisiltite-calcareenites as fillings in the interparticle space.

##### 3.1.4 Quartz

The quartz particles show a terrigenous detrital shape as described by Day-Stírrat et al. (2010) (Fig. 5e). The maximum grain diameter is more than 200 µm and the average size ranges between 20 and 100 µm. Most of grains accumulate in massive calcisiltite-calcareenites, and the rest sporadically occur in interlaminated calcisiltite-calcilutites. Some isolated small terrigenous quartz can be found in the massive calcilutites and the clay-rich laminae of the varve-like laminated calcilutites.

##### 3.1.5 Terrigenous organic matter

Terrigenous organic matters are mainly distributed between the silt grains. They were derived from transport from land with detritus. Other tiny-terrigenous suspended organic matter was deposited with clay, displaying arcuate-like bounding (Lu et al., 2015; Milliken et al., 2013) (Fig. 5f). They were preserved in the micrite matrix.

**Table 2** Summary of the fine-grained carbonate rocks and carbonate rudstones in the Shulu sag

Lithofacies	Description	Compositions (wt. %)			TOC (%)	$\delta^{13}\text{C}$ (‰)
		Calcite	Dolomite	Clay		
Varve-like laminated calcilitite (LF1)	Dark grey and brownish grey (Fig. 3a), 20 m thick in the core of Well S13. Millimeter-thick rhythmic laminae alternating with different colors, granularity and composition. Calcite-rich laminae are displayed as two main types: (1) fining upward, with lightly colored, coarser crystals in the lower region and darkly colored, finer crystals in the upper region (Figs. 4a, 4b); and (2) homogeneous fine calcite laminae (Fig. 4c). Clay-rich laminae are present as two types: (1) darkly coloured with relatively high organic matter and pyrite contents; and (2) lightly colored with relatively low organic matter content and high amounts of clastic particles. Rare bioclasts	65.9 (61) 28.0–93.0	10.6 (61) 2.0–33.0	9.3 (61) 2.0–30.0	2.20 (61) 0.86–5.54	2.8 (61) 1.9–4.1
Graded laminated calcilitite (LF2)	Dark-grey colored, several centimeters up to tens of centimeters thick in Well S13. The thickness of single layers ranges between several millimeters and a few centimeters (Fig. 3b). Normal grading layer and non-rhythmic laminae (Fig. 4d) are indicated by alternating silt-rich and silt-poor laminae. Local bioturbation. Rare bioclasts. Intercalated in LF1	52.3 (66) 22.0–92.0	18.0 (66) 3.0–53.0	12.5 (66) 2.0–29.0	1.44 (66) 0.45–2.25	1.8 (21) –0.3–3.7
Interlaminated calcisiltite-calcilitite (LF3)	Light-grey colored (Fig. 3c), dozens of centimeters thick in Well S13. Normal grading silt layers with low-angle, wispy cross-lamination (Fig. 3c). Liquefaction deformation structures and local bioturbation. Rare bioclasts. Intercalated in LF2 and rudstones	39.8 (34) 19.0–66.0	37.2 (34) 12.0–76.0	10.3 (34) 3.0–25.0	1.00 (34) 0.08–2.71	0.4 (6) –0.6–1.9
Massive calcilitite (LF4)	Darkly colored (Fig. 3d), several meters to 10 m-thick single layers in Well S13. Bulk sample compositions are the same as in LF1. Structureless, no lamination (Figs. 4f, 4g). Rare bioturbation. Local ostracod shells, fish remains and plant fragments. A few sub-rounded carbonate gravels are present as rafts (Fig. 3e). Intercalated in LF2 and LF3	61.4 (50) 27.0–88.0	14.6 (50) 5.0–37.0	9.2 (50) 3.0–19.0	1.69 (50) 0.82–5.41	1.9 (9) 0.9–3.0
Massive calcisiltite-calcarenite (LF5)	Greyish-green colored (Fig. 3f), 15 m thick in Well S13. Low calcite and organic matter contents. Low $\delta^{13}\text{C}$ . High quartz content. Structureless, no lamination (Figs. 4h, 4i). Rare bioturbation. Rare bioclasts. Close to the carbonate rudstones	35.7 (20) 1.0–79.0	20.6 (20) 3.0–68.0	19.3 (20) 9.0–35.0	0.10 (20) 0.08–0.14	–3.4 (7) –4.9––2.8
Clast-supported carbonate rudstone (LF6)	Light-grey colored, generally tens of meters to 100 m thick in the core of Well S13. Carbonate lithoclasts from Palaeozoic strata, including bioclastic limestone, oolitic limestone, edgewise limestone, micritedolostone, and coarse-crystalline dolostone, with rare chert and mudstone. Sequence III mainly contains dolomitic rudstones. Sequence I mainly contains calcareous rudstones. Angular to sub-angular (Fig. 3g), several centimeters up to 60 cm in size. Gradation to LF7	39.5 (92) 1.0–94.0	54.4 (92) 2.0–99.0	3.9 (92) 1.0–11.0	3.1 (92) 1.0–18.0	/
Matrix-supported carbonate rudstone (LF7)	Grey to dark grey, generally tens of centimeters up to several meters in the core of Well S13. Similar clast components as in LF6. Sub-angular to sub-rounded clasts, several centimeters up to 20 cm in size. Matrix-supported textures display calcareous particles with variable clay contents (Fig. 3h). Intercalated in LF6 and LF8	60.7 (8) 34.4–94.0	21.1 (8) 3.0–47.0	10.3 (8) 2.0–18.0	7.9 (8) 1.0–17.0	/
Mixed-source carbonate rudstone (LF8)	Grey to dark grey, generally several centimeters up to several meters in the core of Well S13. Carbonate clasts, including sub-rounded to rounded, fine-gravel to silt size extrabasinal clasts as in LF6 and LF7, and rounded or long striped intrabasinal clasts (Fig. 3i). Intercalated in LF7 and LF3	58.7 (6) 46.0–86.0	25.2 (6) 5.0–35.0	5.7 (6) 4.0–7.0	10.6 (6) 5.0–13.0	/

The number is presented in the form of  $\frac{\text{ave. (num.)}}{(\text{min.} - \text{max.})}$



### 3.2 Biogenic Components

#### 3.2.1 Micritic calcite

Micritic calcite particles, which are smaller than 10  $\mu\text{m}$  in size, are the predominant components of the fine-grained rocks and exist in two forms. The first exists in pure calcite laminae with poorly visible inter-crystal pores (Fig. 6a). Some laminae fine upward, with coarse calcite ( $>4 \mu\text{m}$ ) sub-laminae in the lower regions and fine calcite (2–4  $\mu\text{m}$ ) sub-laminae in the upper regions (Figs. 4a, 4b, 6a). This phenomenon is similar to the calcite layers in the Iberian Karst Lakes (Valero-Garcés et al., 2014). Most of these grains display no perfect rhombic crystals (Kelts and Talbot, 1990) and show no distinct biogenic microstructure (Fig. 6b). The edges of the crystals are curve or planar. Some round and elliptic pores (1–3  $\mu\text{m}$ ) can be observed in the micritic calcite particles (Fig. 6c). Organic filaments surround the calcite grains in the calcite laminae (Fig. 6d). The second type of micritic calcites is mixed with clay and organic matter. Very fine ( $<2 \mu\text{m}$ ) micritic calcite occurs in organic matter-rich regions, and fine micritic calcite (2–4  $\mu\text{m}$ ) is distributed around a center hole (Fig. 6e). Multi-fine-grained micrites sometimes comprise coarse calcite grains, and the outline of the aggregation slightly resembles the crystal morphology of a trigonal system (Fig. 6f).

#### 3.2.2 Intraclasts

The intraclasts are composed of micritic calcite grains and

exhibit a lenticular shape with two sharp ends. Most of the intraclasts in the clay matrix have imbricated fabric, which indicates the flow direction (Fig. 7a). The intraclasts were derived from intermittent underflow erosion and the transport of unconsolidated sedimentary layers (Schieber et al., 2010). The larger intraclasts occur in the mixed-source carbonate rudstones (Zheng et al., 2015). Smaller intraclasts predominantly occur in the interlaminated calcisiltite-calcilutites. Some of the intraclasts occur in the graded laminated calcilutites (Fig. 7b), which indicates the stronger energy of the flow. These materials also exist in the massive calcilutites, which display the nondirective distribution compared to other materials.

#### 3.2.3 Other biogenic materials

The bioclasts and plankton-derived organic matter can be observed. Relatively complete ostracod fossils can be found in Well J94, which is located in the mid-upper western slope. These fossils exhibit a fiber structure and are composed of aragonite (Figs. 7c, 7d). However, only broken debris of ostracod fossils are observed in the massive calcilutites (Fig. 4f) in wells of St1h and St3, which are located near the central sub-sag. No ostracod fossils are present in the other lithofacies. The plankton-derived organic matter constitutes the main hydrocarbon producers in the study area and exhibits a short amorphous shape under stronger fluorescent light (Fig. 4g). Thus, the predominant kerogen types in the fine-grained carbonate rocks include Type I and Type II (Zhao et al., 2014).

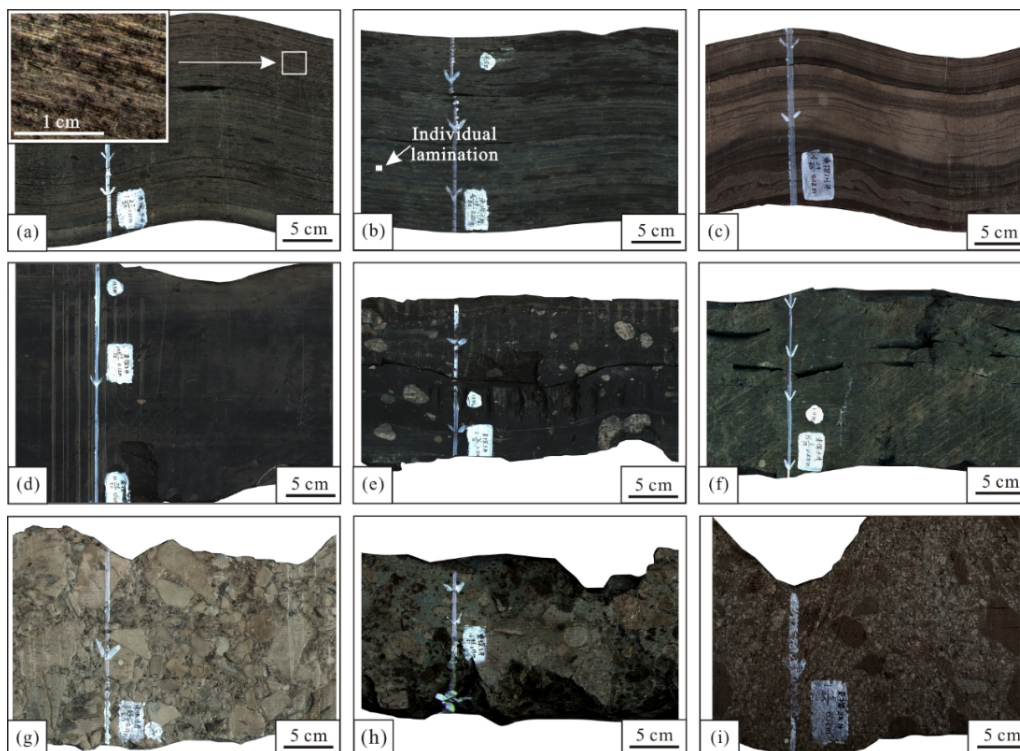


**Figure 3.** Scanned core photos of lithofacies in the Shulu sag. (a) Varve-like laminated calcilutites with fine laminae, from Well St3 at 3 673.85 m; (b) graded laminated calcilutites with millimeter-scale laminae, from Well St3 at 3 813.62 m; (c) interlaminated calcisiltite-calcilutites that exhibit millimeter- and centimeter-scale laminae of altering lightly colored calcisiltite and darkly colored calcilutite couplets, from Well St1h at 3 972.55 m; (d) massive calcilutites, from Well St3 at 3 987.24 m; (e) massive calcilutites that contain floating sub-rounded lithoclasts, from Well St3 at 3 692.9 m; (f) massive calcisiltite-calcarenites that exhibit greyish-green color, from Well St3 at 4 238.82 m; (g) clast-supported carbonate rudstones with poorly sorted and sub-angular dolostone lithoclasts, from Well St3 at 3 911.41 m; (h) matrix-supported carbonate rudstones with sub-rounded lithoclasts and a greyish-green-colored matrix, from Well St3 at 4 268.66 m; (i) mixed-sourced carbonate rudstones, from Well St2x at 4 239.01 m.



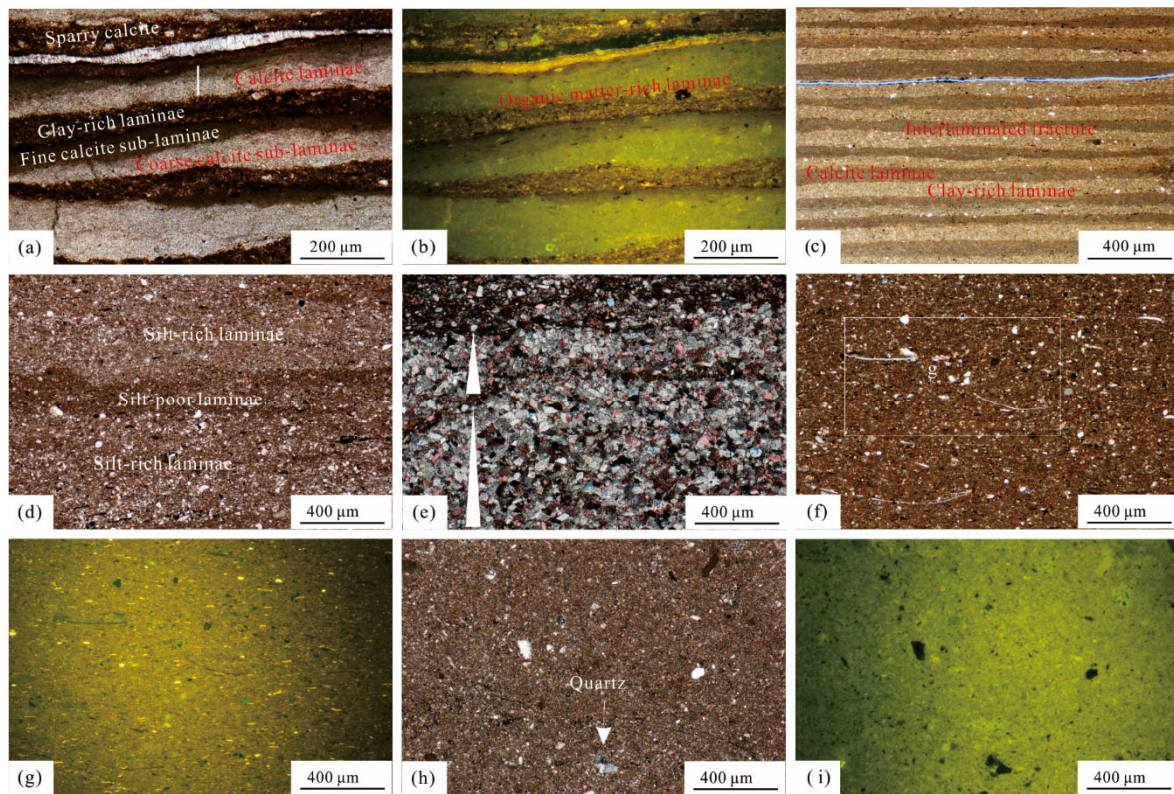


**Figure 4.** Photomicrographs of main fine-grained carbonate rocks. (a)–(b) Varve-like laminated calcilutites that display by alternating calcite-rich and clay-rich couplets, note the sparry calcite lamina on the organic matter-rich lamina, planar-polarized light and incident ultraviolet light, from Well St1h at 4 206.6 m; (c) varve-like laminated calcilutites, planar-polarized light, from Well St3 at 3 684.03 m; (d) graded laminated calcilutites with non-regular lamination, planar-polarized light, from Well St3 at 3 671.69 m; (e) interlaminated calcisiltite-calcilutites that are composed of various terrigenous minerals and clasts that fine upward, crossed-polarized light, from Well St3 at 3 806.45 m; (f)–(g) massive calcilutites that are composed of micritic calcite and silt-size clasts with short amorphous organic matter, planar-polarized light and incident ultraviolet light, from Well St3 at 3 821.49 m; (h)–(i) massive calcisiltite-calcarenites with rare organic matter and sand-size quartz, crossed-polarized light and incident ultraviolet light, from Well St3 at 3 821.49 m.

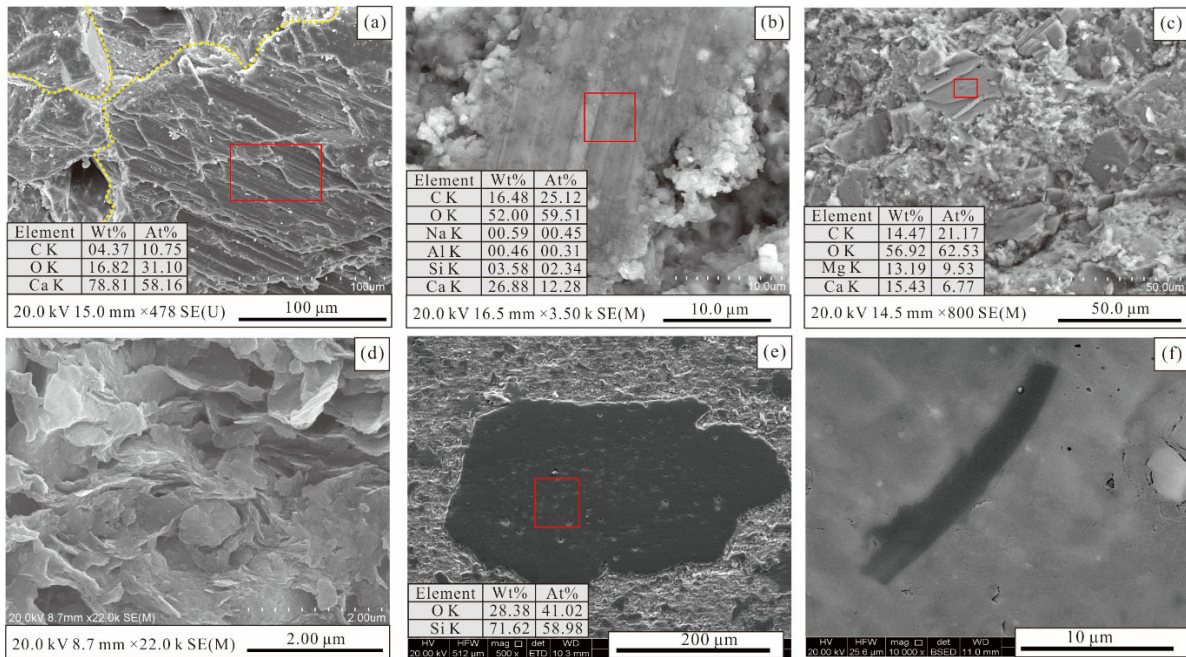


**Figure 5.** SEM photos of terrigenous materials in the Shulu sag. (a) Terrigenous calcite particle from the interlaminated calcisiltite-calcilutites; (b) terrigenous calcareous clasts from the graded laminated calcilutites; (c) terrigenous dolomite grains from the interlaminated calcisiltite-calcilutites; (d) mixed-layer illite/smectite from the clay-rich laminae in the varve-like laminated calcilutites; (e) terrigenous quartz from the massive calcisiltite-calcarenites; (f) wood fragments from the graded laminated calcilutites.



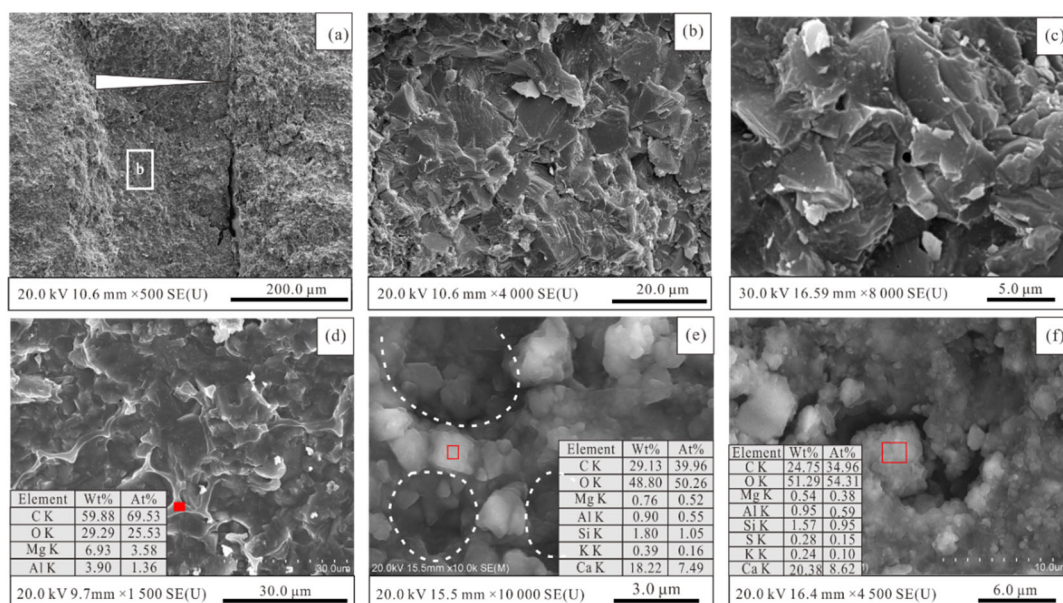


**Figure 6.** SEM photos of endogenic calcite. (a) Calcite-rich laminae that are composed of coarser calcite sub-laminae and finer calcite sub-laminae; (b) subhedral calcite crystals in (a), with curves or planar edges; (c) calcite crystals in the calcite-rich laminae, which contain holes that are of 1–3 μm in diameter; (d) organic filaments in calcite-rich laminae; (e) very fine micritic calcite around a center hole in the massive calcilutites; (f) aggregation of micritic calcite in massive calcilutites.

### 3.3 Diagenetic Components

#### 3.3.1 Sparry calcite

Sparry calcite crystals, which display equant or fibrous forms as described by Zhang et al. (2016), occur as veins in the varve-like laminated calcilutites. These crystals are commonly larger than sedimentary micritic calcite grains. The crystals adjoin to organic matter-rich clay laminae and retain residual black hydrocarbon materials (Figs. 4a, 4b).

#### 3.3.2 Pyrite

Pyrite occurs in the studied fine-grained carbonate rocks as single or clustered framboids (Fig. 7e), which represent an anoxic early diagenesis environment (Aplin and Macquaker, 2011; Taylor and Macquaker, 2000; Wilkin et al., 1996). Most of these minerals exist in clay-rich locations, such as clay laminae in the varve-like laminated calcilutites and mottled clay aggregates in the massive calcilutites. Some can be observed in the center holes of biogenic materials.

#### 3.3.3 Microcrystalline dolomite

In addition to silt-size terrigenous dolomite detritus, some mud-size dolomite crystals can be found in the fine-grained carbonate rocks, with relatively complete crystal forms (Fig. 7f). These crystals are the minority in the rocks. Both of these materials occur in clay-rich locations. Some crystals are surrounded by crumpled sheet mixed layer illite/smectite (Fig. 7f).

### 3.4 Compositions and Isotopes

#### 3.4.1 Compositional differences in the lithofacies

The bulk rock X-ray diffraction of the fine-grained carbonate rocks indicated that most of the calcite is present in varve-like laminated calcilutites and massive calcilutites (Table 2). The calcite content gradually decreased from the graded laminated calcilutites and interlaminated calcisiltite-calcilutites to massive

calcisiltite-calcarenites. The interlaminated calcisiltite-calcilutites and massive calcisiltite-calcarenites have relatively high dolomite contents (Table 2). The other fine-grained carbonate rocks have low dolomite contents. The calcite content in the rudstones depended on the lithology of the source rocks and variable intrabasinal contents. Most of the clast-supported carbonate rudstones have a relatively low calcite content and a higher dolomite content according to the bulk rock analysis (Table 2). Because most of the cores were derived from the upper sequences (i.e., Sequence III), which mainly comprise dolomitic rudstones (Fig. 8). In contrast, some clast-supported carbonate rudstones were taken from the lower sequences (i.e., Sequence I), which predominantly comprise limestone. Although the calcite contents of the clast-supported carbonate rocks varied, most of the matrix-supported carbonate rudstones and mixed-source carbonate rudstones have a relatively higher calcite content (Table 2).

Quartz and clay are minor components of the rocks in the Shulu sag (Table 2). These minerals predominantly occur in massive calcisiltite-calcarenites. The organic matter content can be indicated by the TOC. The pyrolysis analysis showed that the TOC values have a positive correlation with the calcite contents in the fine-grained carbonate rocks (Table 2).

#### 3.4.2 Stable carbon isotopes

The  $\delta^{13}\text{C}$  value was analyzed by the bulk rock dissolution method because separating carbonate grains from different sources in the calcilutites is difficult. However, the  $\delta^{13}\text{C}$  values can be considered as a function of different inorganic carbon sources; therefore, they can indicate the features of the main carbon source because the stable carbon isotope are affected by various physical and bio-chemical processes (Gierlowski-Kordesch, 2010; Bright et al., 2006). These values have a positive correlation with the calcite contents and TOC values (Table 2). In contrast, they have a negative correlation with the other components.



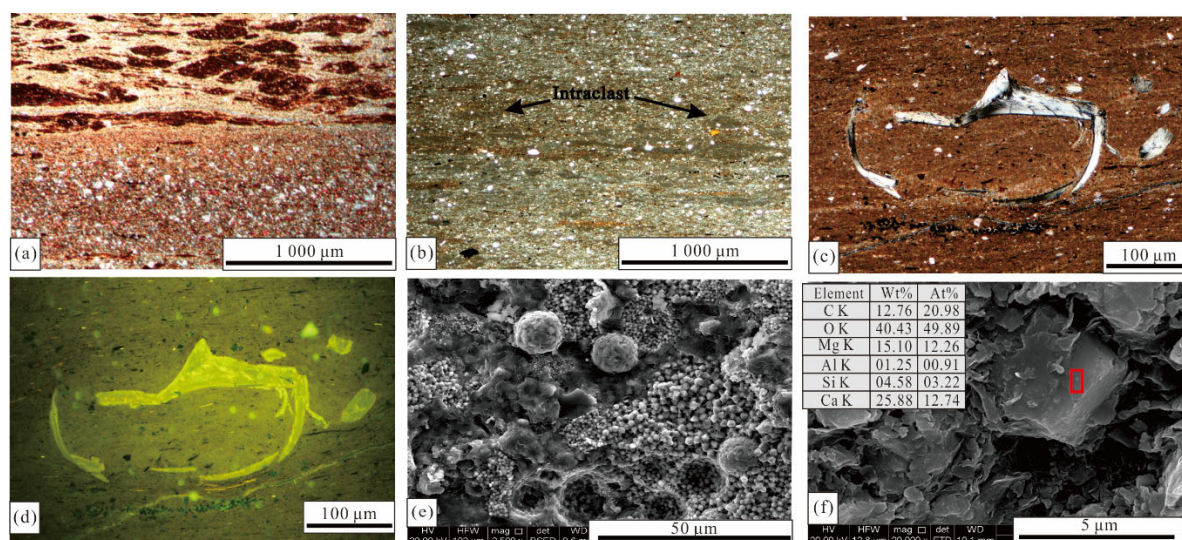


**Figure 7.** (a) Intraclasts with the imbricated fabric, planar-polarized light, from the interlaminated calcisiltite-calcilutites in Well St3 at 3 797.77 m; (b) intraclasts planar-polarized light, from the graded laminated calcilutites in Well St3 at 3 807.76 m; (c)–(d) fossil fragments in the massive calcilutites, crossed-polarized light and incident ultraviolet light, from Well J94 at 3 113.89 m; (e) clustered pyrite framboids; (f) microcrystalline dolomite that is surrounded by mixed-layer illite/smectite.

### 3.5 Vertical Stacking Patterns

The lower member of  $E_{S3}$  in the Shulu sag can be divided into five sequences (Zheng et al., 2015). Most of the carbonate rudstones occurred extensively in the LST of Sequence I on the western slope (Fig. 8). However, they occurred locally in the TST or HST of Sequence I in Well J97 (Fig. 8). The lake region was narrow during the initial stage of basin evolution (Jiang et al., 2007). These rudstones are characterized by a normal or inverse grading sequence, which comprise relatively smaller, sub-rounded carbonate lithoclasts and locally exhibit inconspicuous imbricate arrangements as coarse-grained fan-deltas (McPherson et al., 1987). Organic matter-poor, and greyish-green massive calcisiltite-calcarenites occurred in Sequence I and gradated toward the organic matter-rich, dark-grey, and fine-grained carbonate rocks (Fig. 8), indicating that the lake area deepened and expanded. During this stage, the main lithologies of source area were Ordovician limestones; therefore, the carbonate rudstones of the sequence have a higher calcite content (Fig. 8).

During Sequence II, carbonate rudstones mainly occurred in the LST, and some mixed-source carbonate rocks occurred in the HST (Fig. 8). Varve-like laminated calcilutites and massive calcilutites were the predominant components in the TST and HST, respectively (Fig. 8).

The carbonate rudstones in Sequence III are characterized by thick, brecciated clast-supported carbonate rudstones (i.e., Well St3) and mixed-source carbonate rudstones (i.e., Well St1h) (Fig. 8). Compared with the rudstones in Sequence I, these rudstones had a limited distribution with larger, angular carbonate lithoclasts and exhibited normal grading or massive sequences. During this stage, the main lithology in the Ningjin uplift was Cambrian dolostones, and therefore, the rudstones of the sequence were predominantly comprised dolostone clasts. During the deepening stage, the basin was filled with massive calcilutites, graded laminated calcilutites and interlaminated calcisiltite-calcilutites (Fig. 8). These fine-grained carbonate rocks contained more clay and quartz components than those in Sequence II. However, compared with the fined-grained carbonated rocks in

Sequence II, their TOC values and calcite content are lower.

During sequences IV and V, the lake area further expanded and alluvial fans rarely occurred along in the western slope (Fig. 8). The characteristics of the fine-grained carbonate rocks were inherited from Sequence III, including the low organic matter and calcite contents. Varve-like laminated calcilutites with higher calcite content and TOC value occurred during the early stage of Sequence V (Fig. 8). Later, the calcite contents and TOC of the fine-grained carbonate rocks decreased again.

## 4 DISCUSSION

### 4.1 Origin of the Calcite

Lacustrine calcite particles can be derived from terrigenous clast transport and biologically induced or controlled precipitation (Jiang et al., 2007; Kelts and Talbot, 1990; Kelts and Hsü, 1978). However, distinguishing between extrabasinal and intrabasinal calcite remains a problem. The calcite laminae in the varve-like laminated calcilutites are completely composed by calcite grains (Fig. 6a), which indicate that these grains were not transported from an extrabasin or shallow lake; otherwise, the lamination would comprise other minerals as with the graded laminations in the interlaminated calcisiltite-calcilutites (Fig. 4e). Most of the micritic calcite grains in both the calcite laminae and massive mixed matrix contain sub-micron holes in the crystals, which are a sign of the cyanobacteria-induced calcite (Chafetz, 2013; Stabel, 1985). The contrast tests that were conducted by Dittrich et al. (2003) suggested that the cell walls of cyanobacteria acted as the substrate of calcite nucleation. These holes are the products of organism degradation during burial (Dittrich et al., 2004). The filaments of organisms around calcite grains are similar to extracellular polysaccharides (Pacton et al., 2007; Dittrich et al., 2003). These features indicate that picoplankton may have served a vital role in the micritic calcite precipitation in the study area. The photosynthesis of algae in the epilimnion can remove  $CO_2$ , increase pH and shift the equilibria towards  $CO_3^{2-}$  species, which can create a micro-environment with supersaturation (Kelts and Hsü, 1978). The high

temperature in the summer can influence primary productivity and decrease the solubility products to indirectly affect calcite precipitation (Hodell et al., 1998).

Carbon isotopes can also be utilized to deduce differences in extrabasinal and intrabasinal calcite and judge the primary productivity of a lake (Griffiths et al., 2002; Hodell et al., 1998) because the  $\delta^{13}C$  can indicate information of the dissolved inorganic carbon (DIC) in the epilimnion (Leng and Marshall, 2004) and the carbonate clasts (Bright et al., 2006). The  $\delta^{13}C$  of the DIC is controlled by biological photosynthesis and exchange  $CO_2$  between the atmosphere and lake (Kelts and Talbot, 1990; Lee et al., 1987). Most of the fine-grained carbonate rocks have high carbon isotope values (Table 2). However, the  $\delta^{13}C$  of the

carbonate rudstones in the study area is low and ranges between -3‰ to 0.5‰ (Qiu et al., 2010).

Therefore, coarse- and fine-grained carbonate rocks obviously had different material sources. The  $\delta^{13}C$  of the Cambro-Ordovician marine carbonates in the Bohai Bay Basin ranges from -7.6‰ to 1.6‰ (Wang and Feng, 2002). If these rocks were presumably completely composed by terrigenous clasts, they would exhibit  $\delta^{13}C$  values in the range of the lower Paleozoic strata, such as those of the carbonate rudstones in the Shulu sag (Qiu et al., 2010). This difference in  $\delta^{13}C$  values indicates a change in the ratio from terrigenous to endogenic carbonates. Therefore, the  $\delta^{13}C$  of the bulk rock should be higher with a greater percentage of biologically induced calcite.

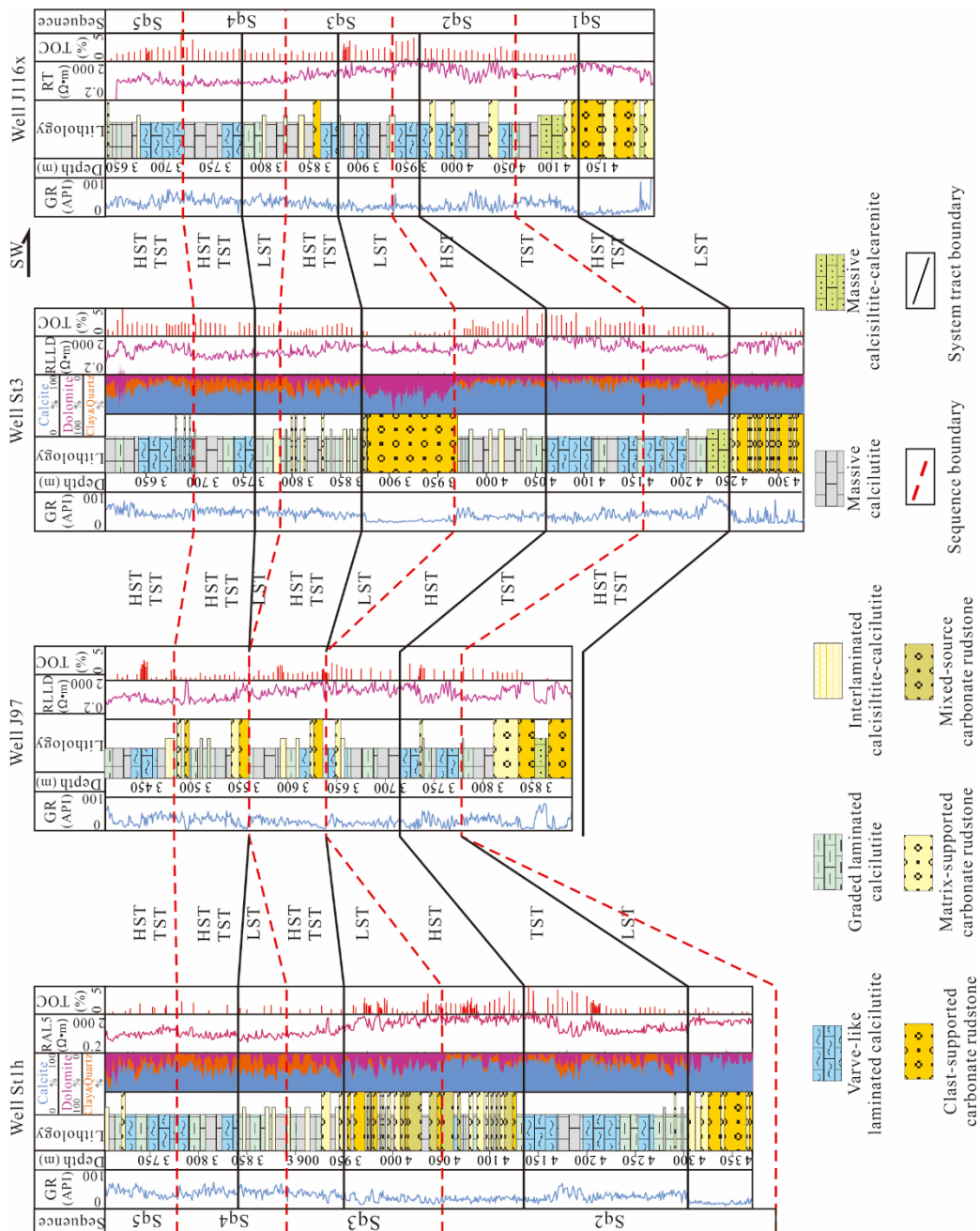


**Figure 8.** Correlation of the lithofacies association sequences and stratigraphic framework. This section is marked by the red dash line in Fig. 2b, LST. low stand systems tract, TST. transgressive systems tract, HST. high stand systems tract.

Some calcite formed during burial in addition to terrigenous and biologically induced calcite. One type of diagenetic calcite derived from pressure-solution was observed between silt-size carbonate grains. Pressure-solution can increase the amount of dissolved carbonate and provide a new source for carbonate cement (Flügel, 2004). The other type is related to hydrocarbon generation and expulsion (Cobbold et al., 2013). Organic matter-rich clay laminae could have released organic acid in the oil generation window. These acidic materials could have dissolved sedimentary micrites along the interlayer space. The freed cations then in turn aggregated in situ and precipitated to form sparry calcite (Zhang et al., 2016).

#### 4.2 Origin of Other Materials

Dolomite occurred in both the source area and lacustrine sediments as calcite. Two main types of dolomites were found: (1) coarse rhombic dolomites and (2) microcrystalline dolomites. The brecciated dolostones comprising coarse rhombic dolomite occurred in Sequence III, representing the lithology of the catchments during the period. In the same sequence, worn rhombic dolomite grains occurred in interlaminated calcisiltite-calcilutites, which exhibited the same habits as in the carbonate rudstones. Similar terrigenous dolomite detritus have been observed in Sarliève lacustrine deposits (Fourmont et al., 2009).

Microcrystalline dolomite occurred in clay-rich deposits. This dolomite was surrounded by mixed-layer illite/smectite. Its origin was difficult to determine because no unequivocal proof can be obtained from their crystal habits. This mineral had no ability to influence the  $\delta^{13}\text{C}$  because of their scarce presence in the deposits. No extensive primary or diagenetic dolomite occurred in the fine-grained carbonate rocks, which indicate that the pH or the Mg/Ca ratio was insufficient (Casado et al., 2014; Kelts and Hsü, 1978). Mg-rich clay can release a certain amount of  $\text{Mg}^{2+}$  into the pore water, which creates a favorable microenvironment for forming dolomite crystals (Casado et al., 2014; Bustillo and Alonso-Zarza, 2007). Thus, the isolated microcrystalline may have been derived from burial diagenesis during the transformation of clay minerals.

The quartz and clay were derived from terrigenous detritus and mainly accumulated in fine-grained carbonate rocks. However, these minerals had a negative relationship with calcite. These siliciclastic detritus are interpreted as the residuum of surrounding weathered soil (Macquaker et al., 2007). During the initial stage of basin evolution, abundant weathered quartz and clay gathered in the basin because the lake was shallow, and most of the siliciclastic detritus directly settled with terrigenous clastic carbonate. Thus, the clay- and quartz-rich massive calcisiltite-calcarenites exhibited low  $\delta^{13}\text{C}$  and a greyish-green color. As the lake basin expanded, the siliciclastic detritus and calcite started to settle out separately. Micritic calcite mainly precipitated in the thermally stratified water columns of the lake during the hot season as discussed above. However, most of the fine-grained siliciclastic detritus remained in suspension in the thermocline (Sturm and Matter, 1978) and would settle out as a "suspension blanket" after water column turnover during the cold season (Sturm and Matter, 1978). Thus, the varve-like laminated calcilutites gained laminae with different compositions. When these early sediments were eroded and transported into the

deeper lake region, all of the minerals and clasts would be mixed and redeposited together.

#### 4.3 Origin of Lithofacies

The varve-like laminated calcilutites, which comprised lightly and darkly colored laminae with varying colors, grain sizes and compositions, indicate alternating depositional mechanisms that were controlled by seasonal variation and variable input sources (Glenn and Kelts, 1991). Lacustrine sediments that are not destroyed by bioturbation or physical disturbance can exhibit seasonal textures (Anderson and Dean, 1988; Anderson, 1986). Analogous annual laminated sediments have been found in Iberian Karst lakes (Valero-Garcés et al., 2014) and in Lake Yoa (Francus et al., 2013). The high  $\delta^{13}\text{C}$  and calcite contents indicate that the biologically induced calcites were the predominant component of the rocks as discussed above. The differences in grain size within the calcite laminae may hint at changes in the environment. The larger calcite probably formed during the spring because of relatively lower supersaturation (Kelts and Hsü, 1978) or phosphate consumption caused by photosynthetic activity (Teranes et al., 1999). The smaller calcite might have precipitated during the hot summer with higher supersaturation or primary productivity (Valero-Garcés et al., 2014; Kelts and Hsü, 1978). The settlement of organic matter occurred during the cold season with fine-grained detritus (Zolitschka, 2007). Under anoxic conditions, sedimentary organic matter can be well protected, and dissolved sulphate can be reduced to sulphide (i.e., pyrite) by microorganisms (Zolitschka et al., 2015); therefore, the clay-rich lamina has a darker-color. When the annual organic productivity was lower or the detritus input was abundant, the clay-rich lamina would display a light color and rare pyrite.

The interlaminated calcisiltite-calcilutites primarily comprised terrigenous detritus. Lamination with alternating silt- and clay-size sub-laminae is a common feature of turbidites in the deep lakes (Zhang and Scholz, 2015; Chang and Chun, 2012; Lambert and Hsü, 1979b). The rocks exhibited a normal grading sequence without a coarsening-upward basal unit, which indicates that the rocks may not have been triggered by hyperpycnal flow (Mulder et al., 2003). These silt particle-rich rocks, which display as the abundant soft sediment deformation structures in Sequence III, have been proposed as seismites (Zheng et al., 2015). In turn, seismically induced failure can generate debris flows and further evolve into turbidity currents (Osleger et al., 2009).

The graded laminated calcilutites were mainly intercalated in the interlaminated calcisiltite-calcilutites and exhibited the same normal grading. The compositions and structural features indicate that these rocks are the tail deposition of traditional turbidity currents (Td-Te) or upper fine-grained turbidite sequences (T4-T7) (Stow and Shanmugam, 1980), which involves deposition from low-energy and dilute muddy turbidity currents with decreased terrigenous detritus. Because of the interchange of materials between the turbidity currents and underlying sediments (Lincoln and Pratson, 2000), these new deposits that were derived from the flow body would gradually have a similar composition as normal background sediments.

No obvious layer interfaces and bioturbation structures



were present within the thick-layer massive calcilutites according to visual observation. Similar massive fine-grained rocks, called homogenites or unifites, occur in the deep water area of marine and lake basins (Morellón et al., 2009; Tripsanas et al., 2004; Stanley, 1981). The origin of these homogenous rocks is considered to be related to earthquakes, including seismically induced metaturbidites (Mulder et al., 2009), and fluidization (Beck, 2009). Although the mineral compositions and isotope features of the massive calcilutites indicate that the rocks primarily comprise intrabasinal materials, these rocks also contain a certain amount of silt-size detritus, oriented ostracod shells and plant debris. These features indicate that the massive calcilutites originated from redeposited sediments and that the primary materials were derived from a shallow lake. When an earthquake occurred, the shaking caused the fluidization of unconsolidated sediments in the shallow lake. These sediments would slide down along the slope and evolve into large, dilute turbidity currents and suspended clouds (Cita et al., 2008). This turbulent flow can last several months (Tripsanas et al., 2004) and have a large influence on the water column. When algae bloom, plankton can attach to suspended particles within the suspended cloud. This association can overcome the buoyant force and cause the materials to settle down together in a deep lake to form massive, darkly colored, organic matter-rich calcilutites. Due to the multiple seismic events (Zheng et al., 2015), subsequent earthquakes could have caused the fluidization of early massive sediments and made them thoroughly homogenized. Some massive calcilutites with floating gravel were probably derived from cohesive muddy debris flows (Talling et al., 2012).

Compared with other lithofacies, the color of the massive calcisiltite-calcarenites reflects an oxic depositional environment. In addition, abundant terrigenous clasts (quartz and dolomite) and low  $\delta^{13}\text{C}$  indicate that the deposition was directly controlled by the terrigenous clasts input. The massive structure and sand-size detritus were responded to gravity flow (Myrow and Hiscott, 1991). Consequently, the rocks were deposited in shallow water through slumping.

#### 4.4 Relationship between Fine-Grained Carbonate Rocks and Rudstones

The carbonate rudstones in the Shulu sag were sourced from the Paleozoic strata in the Ningjin uplift and had similar lithological compositions (Jiang et al., 2007) and carbon isotope values (Qiu et al., 2010) as the Mid-Upper Cambro-Ordovician bedrock. These rudstones widely occurred at the bottom of the lake basin and exhibited back-stepped lobes (Jiang et al., 2007). Greyish-green massive calcisiltite-calcarenites formed during the same period because of the dry climate and strong clastic input.

The carbonate rudstones in Sequence III exhibit an isolated distribution in the basin and are considered to be sediments of slump or debris flows that were triggered by earthquakes. The mixed-source carbonate rudstones were considered to have been derived from erosion through the debris flows on the underlying unconsolidated substratum (Zheng et al., 2015). The occurrence of calcilutite intraclasts indicates that the flow transition began between debris flow and turbidity current (Sumner et al., 2009).

Thus, interlaminated calcisiltite-calcilutites were always found in Sequence III, which gradually settled down as the flow decelerated (Stow and Bowen, 1978). The massive calcilutites were also the products of the shaking in the lake basin from earthquakes and mass sliding.

#### 4.5 Controlling Factors for Carbonate Accumulation

Unlike marine carbonates, the formation of lacustrine carbonates is controlled by the lithology of the bedrocks, climate, tectonics and primary productivity (Gierlowski-Kordesch, 2010; Kelts and Talbot, 1990; Kelts and Hsü, 1978). Widespread carbonate rocks in the provenance area could have provided both clasts and calcium to the basin (Jiang et al., 2007; Gierlowski-Kordesch, 1998), which allowed for thick carbonate fillings in the lakes (Jones and Bowser, 1978). The Early Paleozoic marine carbonates that were exposed in the Ningjin uplift could have provided a large amount of carbonate materials to the Shulu sag (Jiang et al., 2007). Thus, the Shulu sag could have accumulated 1 200 m-thick carbonates in the depocenter of the basin (Zheng et al., 2015).

Although climate is not the determining factor in carbonate accumulation (Garcés and Gierlowski-Kordesch, 1994), it controls biogenic productivity and influences the weathering rates and type, which regulate the supply of materials (Romero-Viana et al., 2008; Platt and Wright, 1991). The climate was dry during the initial basin formation stage (Ren, 1986); thus, physical weathering predominated over the provenance area and controlled the lithology of the fills. A shift to a semi-humid and then humid climate (Zhang et al., 2001), which enhanced chemical weathering, could have favoured the formation of fine-grained carbonate rocks through biological photosynthesis.

Tectonic activity could have shaken the lake basin and controlled the formation of lithofacies by reworking early sediments as discussed above. Varve-like laminated calcilutites were only effectivity preserved without strong shaking and the input of terrigenous materials (Zolitschka, 2007). Primary productivity controlled the total amount of micritic calcite precipitation (Hodell et al., 1998) and organic matter. Sequence II had a higher calcite content and TOC values than other sequences because of its relatively higher primary productivity.

#### 4.6 Petroleum Geologic Significance

Although the Shulu sag's fine-grained carbonate rocks exhibit low values of physical properties of reservoirs (porosities between 0.4% and 2.3%, permeabilities between  $0.04 \times 10^{-3}$  and  $3.78 \times 10^{-3} \mu\text{m}^2$ ) (Zhao et al., 2014), they still provided a relatively higher production of oil and gas in Sequence II (Table 1). They are important lithological reservoirs as with the carbonate rudstones reservoirs in the study area (Kong et al., 2016; Han et al., 2015; Zheng et al., 2015; Jiang and Li, 2013). Compared with conventional reservoirs, lithofacies and compositions are the key factors for evaluating the quality of unconventional fine-grained carbonate reservoirs. These factors control the distribution of main reservoir space and influence hydrocarbon accumulation. Varve-like laminated calcilutites contain many micropores and microfissures caused by their special sedimentary textures and mineral compositions. Main types of reservoir space include interparticle pores, intraparticle

pores, organic matter pores and fracture pores in the fine-grained reservoirs (Loucks et al., 2012). Darkly colored, clay-rich laminae have a higher organic matter content. Organic matter can generate effective pore networks by themselves (Loucks et al., 2009) and release organic acid to dissolve carbonate particles (Zhao et al., 2014). Therefore, they mainly contain organic matter pores (Fig. 9a) and dissolution-rim pores of calcite grains (Fig. 9b) (Kong et al., 2016). Lightly colored, clay-rich laminae contains more terrigenous clasts and clay; therefore, their main micropores include intraplatelet pores with clay aggregates (Fig. 9c). Intercrystalline pores within pyrite framboids can be found in all clay-rich laminae (Fig. 9d). Calcite-rich laminae also have good reservoir potential because of their abundance of residual pores from the decay of cells in the crystals (Chafetz, 2013). These pores (Fig. 6c), which are unconnected and sub-micron in size, cannot be detected by a standardized porosity analyser. However, these pores can effectively store oil drops and form hydrocarbon accumulation in the area of microfissures development. In addition to micropores, abnormal high-pressure microfissures (Fig. 9f), which originate from high flow pressure during kerogen decarboxylation (Zhao et al., 2014), and interlamination fissures (Fig. 9e) can be observed in the varve-like laminated calcilutites. They can make up effective seepage networks to connect micropores (Kong et al., 2016). Compared

with varve-like laminated calcilutites, other laminated sediments have poor potential as reservoirs because they have a lower organic matter content. The reservoir quality of massive sediments is also worse than the varve-like laminated calcilutites because they lack effective channels for the migration of hydrocarbons.

Figure 8 shows that the calcite content has a positive correlation with the TOC value in the layer of fine-grained carbonate rocks. Warmer summers and eutrophication conditions can increase the duration of primary production as well as the abundance of plankton, which in turn increased the amount of precipitated calcite (Mullins, 1998). Compared with the other sequences, Sequence II had higher calcite content and TOC value. This phenomenon indicates that the lake basin had higher primary productivity during the rock-formation stage. A large amount of organic matter not only provides hydrocarbon to form oil pool, but also modifies the quality of the reservoirs (Jiang et al., 2014, 2013). Thermal stratification and anoxic bottom water are favourable factors for preserving organic matter and varve-like laminated sediments (Zolitschka et al., 2015; Mullins, 1998). Moreover, varve-like laminated calcilutites are the mainly lithofacies in Sequence II. Therefore, Sequence II has good reservoir potential with high-quality, organic matter-rich lithofacies.

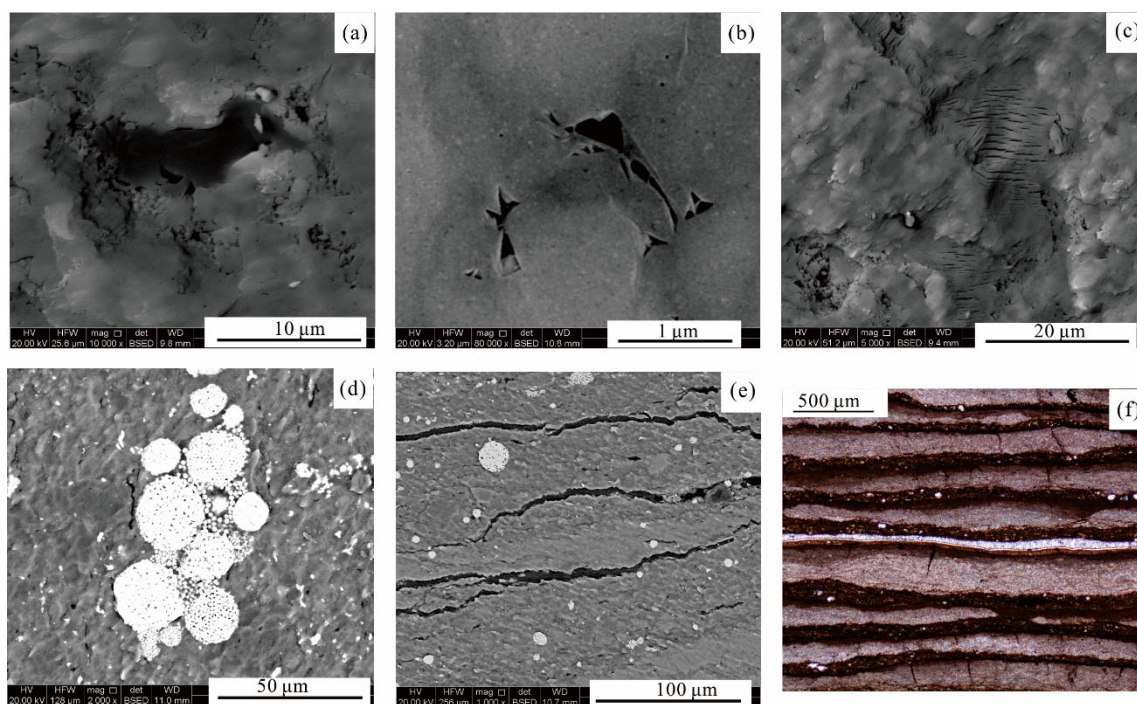


**Figure 9.** Micropores and microfissures of varve-like laminated calcilutites. (a) Organic matter pores (Well St3 at 4 102.33 m); (b) dissolution-rim pores of calcite grains (Well J85 at 3 771.38 m); (c) intraplatelet pores with clay aggregates (Well St3 at 3 681.49 m); (d) intercrystalline pores within pyrite framboids (Well 97 at 3 638.04 m); (e) interlamination fissures (Well J85 at 3782.85 m); (f) abnormal high-pressure microfissures (Well St1h at 4 213.4 m).

## 5 CONCLUSION

The fine-grained carbonate rocks in the Shulu sag comprise extrabasinal and intrabasinal materials. The terrigenous clasts were sourced from Early Paleozoic marine carbonates by mechanical weathering and transported into the lake by gravity flow. The micritic calcite grains were formed through

picoplankton photosynthesis in the epilimnion, and they are characterized by high  $\delta^{13}\text{C}$  and micro-holes in the crystals. The intraclasts were derived from intermittent underflow erosion and the transport of unconsolidated sedimentary substrata. The diagenetic components include sparry calcite, pyrite and dolomite.

They formed at the sediment-water interface or during the burial period. Various components could have been deposited by physical, chemical and biological processes.

The fine-grained carbonate rocks in the Shulu sag can be divided into five lithofacies according to the characteristics of the compositions and structures. Varve-like laminated calcilutites, which comprise lightly and darkly colored laminae with varying colors, grain sizes and compositions, indicate alternating depositional mechanisms that were controlled by seasonal variations and variable input sources. Graded laminated calcilutites and interlaminated calcisiltite-calcilutites were deposited by turbidity flow that was triggered by earthquakes. Massive, thick-bed calcilutites were redeposited by mass transport from fluidized sediments under strong shaking conditions during earthquakes. Massive calcisiltite-calcarenites with low  $\delta^{13}\text{C}$  were deposited in shallow water from slumping.

Physical weathering predominated over the provenance area because of the dry climate during the initial stage of basin evolution; thus, carbonate rudstone alluvial fans occurred widely in the basin with massive calcisiltite-calcarenites. The change from an arid to humid climate enhanced chemical weathering, leading to the deposition of abundant varve-like laminated calcilutites in the deep lake by biological processes. When tectonic activity was widespread and earthquakes occurred, a large amount of terrigenous clasts were transported into the lake by debris flows and turbidity currents. Silt-size clast-rich sediments accumulated in the deep lake, and early sediments were reworked by shaking in the lake basin. In addition to the lithology of the bedrocks, tectonics and climate, primary productivity was an important factor controlling carbonate accumulation. The amounts of biologically induced calcite increased with higher primary productivity.

The sedimentology of the Shulu sag's fine-grained carbonate rocks suggests that the material compositions of the lithofacies can influence the nature of the rocks. Lithofacies and compositions are the key factors for evaluating the quality of unconventional fine-grained carbonate reservoirs. Thus, this study provides clues for understanding the sedimentary origins of fine-grained carbonate rocks and for evaluating potential of fine-grained carbonate reservoirs.

## ACKNOWLEDGMENTS

The finances for this study were provided by the National Major Research Program for Science and Technology of China (No. 2017ZX05009-002) and the National Natural Science Fund (No. 41772090). We are grateful to the Huabei (North China) Oil Company for permitting data access. The final publication is available at Springer via <https://doi.org/10.1007/s12583-016-0927-x>.

## REFERENCES CITED

- Anadón, P., Utrilla, R., Vázquez, A., 2000. Use of Charophyte Carbonates as Proxy Indicators of Subtle Hydrological and Chemical Changes in Marl Lakes: Example from the Miocene Bicorn Basin, Eastern Spain. *Sedimentary Geology*, 133(3/4): 325–347. [https://doi.org/10.1016/S0037-0738\(00\)00047-6](https://doi.org/10.1016/S0037-0738(00)00047-6)
- Anderson, R. Y., 1986. The Varve Microcosm: Propagator of Cyclic Bedding. *Paleoceanography*, 1(4): 373–382. <https://doi.org/10.1029/pa001i004p00373>
- Anderson, R. Y., Dean, W. E., 1988. Lacustrine Varve Formation through Time. *Palaeogeography, Palaeoclimatology, Palaeoecology*, 62(1–4): 215–235. [https://doi.org/10.1016/0031-0182\(88\)90055-7](https://doi.org/10.1016/0031-0182(88)90055-7)
- Aplin, A. C., Macquaker, J. H. S., 2011. Mudstone Diversity: Origin and Implications for Source, Seal, and Reservoir Properties in Petroleum Systems. *AAPG Bulletin*, 95(12): 2031–2059. <https://doi.org/10.1306/03281110162>
- Beck, C., 2009. “Late Quaternary Lacustrine Paleo-Seismic Archives in North-Western Alps: Examples of Earthquake-Origin Assessment of Sedimentary Disturbances”. *Earth-Science Reviews*, 96(4): 327–344. <https://doi.org/10.1016/j.earscirev.2009.07.005>
- Behrens, E. W., 1984. Unifite Muds in Intraslope Basins, Northwest Gulf of Mexico. *Geo-Marine Letters*, 4(3/4): 227–233. <https://doi.org/10.1007/bf02281711>
- Bright, J., Kaufman, D. S., Forester, R. M., et al., 2006. A Continuous 250 000 yr Record of Oxygen and Carbon Isotopes in Ostracode and Bulk-Sediment Carbonate from Bear Lake, Utah-Idaho. *Quaternary Science Reviews*, 25(17/18): 2258–2270. <https://doi.org/10.1016/j.quascirev.2005.12.011>
- Bustillo, M. A., Alonso-Zarza, A. M., 2007. Overlapping of Pedogenesis and Meteoric Diagenesis in Distal Alluvial and Shallow Lacustrine Deposits in the Madrid Miocene Basin, Spain. *Sedimentary Geology*, 198(3/4): 255–271. <https://doi.org/10.1016/j.sedgeo.2006.12.006>
- Casado, A. I., Alonso-Zarza, A. M., la Iglesia, Á., 2014. Morphology and Origin of Dolomite in Paleosols and Lacustrine Sequences. Examples from the Miocene of the Madrid Basin. *Sedimentary Geology*, 312(10): 50–62. <https://doi.org/10.1016/j.sedgeo.2014.07.005>
- Chafetz, H. S., 2013. Porosity in Bacterially Induced Carbonates: Focus on Micropores. *AAPG Bulletin*, 97(11): 2103–2111. <https://doi.org/10.1306/04231312173>
- Chang, C. Y., 1991. Geological Characteristics and Distribution Patterns of Hydrocarbon Deposits in the Bohai Bay Basin, East China. *Marine and Petroleum Geology*, 8(1): 98–106. [https://doi.org/10.1016/0264-8172\(91\)90048-6](https://doi.org/10.1016/0264-8172(91)90048-6)
- Chang, T. S., Chun, S. S., 2012. Micro-Characteristics of Sustained, Fine-Grained Lacustrine Turbidites in the Cretaceous Hwangsan Tuff, SW Korea. *Geosciences Journal*, 16(4): 409–420. <https://doi.org/10.1007/s12303-012-0042-3>
- Charles, M. J., Simmons, M. S., 1986. Methods for the Determination of Carbon in Soils and Sediments: A Review. *The Analyst*, 111(4): 385. <https://doi.org/10.1039/an9861100385>
- Cita, M., 2008. Deep-Sea Homogenites: Sedimentary Expression of a Prehistoric Megatsunami in the Eastern Mediterranean. In: Shiki, T., Tsuji, Y., Minoura, K., eds., Tsunamiites—Features and Implications. Elsevier, Amsterdam. 185–202
- Cobbold, P. R., Zanella, A., Rodrigues, N., et al., 2013. Bedding-Parallel Fibrous Veins (Beef and Cone-in-Cone): Worldwide Occurrence and Possible Significance in Terms of Fluid Overpressure, Hydrocarbon Generation and Mineralization. *Marine and Petroleum Geology*, 43(4): 1–20. <https://doi.org/10.1016/j.marpetgeo.2013.01.010>
- Day-Stirrat, R. J., Dutton, S. P., Milliken, K. L., et al., 2010. Fabric Anisotropy Induced by Primary Depositional Variations in the Silt: Clay Ratio in Two Fine-Grained Slope Fan Complexes: Texas Gulf Coast and Northern North Sea. *Sedimentary Geology*, 226(1/2/3/4): 42–53. <https://doi.org/10.1016/j.sedgeo.2010.02.007>
- Dean, W. E., 1981. Carbonate Minerals and Organic Matter in Sediments of Modern North Temperate Hard-Water Lakes. In: Ethridge, F. G., Flores, R. M., eds., Recent and Ancient Non-Marine Depositional Environments: Models for Exploration. *SEPM Special Publication*, 31: 213–231
- Dean, W., Rosenbaum, J., Skipp, G., et al., 2006. Unusual Holocene and Late



- Pleistocene Carbonate Sedimentation in Bear Lake, Utah and Idaho, USA. *Sedimentary Geology*, 185(1/2): 93–112. <https://doi.org/10.1016/j.sedgeo.2005.11.016>
- Dittrich, M., Kurz, P., Wehrl, B., 2004. The Role of Autotrophic Picocyanobacteria in Calcite Precipitation in an Oligotrophic Lake. *Geomicrobiology Journal*, 21(1): 45–53. <https://doi.org/10.1080/01490450490253455>
- Dittrich, M., Müller, B., Mavrocordatos, D., et al., 2003. Induced Calcite Precipitation by Cyanobacterium *Synechococcus*. *Acta Hydrochimica et Hydrobiologica*, 31(2): 162–169. <https://doi.org/10.1002/ahch.200300486>
- Flügel, E., 2004. *Microfacies of Carbonate Rocks: Analysis, Interpretation and Application*. Springer, New York. 314–321
- Fourmont, A., Macaire, J. J., Bréhéret, J. G., 2009. Contrasted Late Glacial and Holocene Hydrology of Sarliève Paleolake (France) from Sediment Geometry and Detrital Versus Biochemical Composition. *Journal of Paleolimnology*, 41(3): 471–490. <https://doi.org/10.1007/s10933-008-9238-y>
- Francus, P., von Suchodoletz, H., Dietze, M., et al., 2013. Varved Sediments of Lake Yoa (Ounianga Kebir, Chad) Reveal Progressive Drying of the Sahara during the Last 6 100 Years. *Sedimentology*, 60(4): 911–934. <https://doi.org/10.1111/j.1365-3091.2012.01370.x>
- Freytet, P., Verrecchia, E. P., 2002. Lacustrine and Palustrine Carbonate Petrography: An Overview. *Journal of Paleolimnology*, 27(2): 221–237
- Garcés, B. L. V., Gierlowski-Kordesch, E. H., 1994. Lacustrine Carbonate Deposition in Middle Pennsylvanian Cyclothems? The Upper Freeport Formation, Appalachian Basin, USA. *Journal of Paleolimnology*, 11(1): 109–132. <https://doi.org/10.1007/bf00683273>
- Gierlowski-Kordesch, E. H., 1998. Carbonate Deposition in an Ephemeral Siliciclastic Alluvial System: Jurassic Shuttle Meadow Formation, Newark Supergroup, Hartford Basin, USA. *Palaeogeography, Palaeoclimatology, Palaeoecology*, 140(1/2/3/4): 161–184. [https://doi.org/10.1016/s0031-0182\(98\)00039-x](https://doi.org/10.1016/s0031-0182(98)00039-x)
- Gierlowski-Kordesch, E. H., 2010. Lacustrine Carbonates. *Developments in Sedimentology*, 61(1): 1–101
- Glenn, C., Kelts, K., 1991. Sedimentary Rhythms in Lake Deposits. In: Einsele, G., Ricken, W., Seilacher, A., eds., *Cycles and Events in Stratigraphy*. Springer, Berlin. 188–221
- Griffiths, S. J., Street-Perrott, F. A., Holmes, J. A., et al., 2002. Chemical and Isotopic Composition of Modern Water Bodies in the Lake Kopais Basin, Central Greece: Analogues for the Interpretation of the Lacustrine Sedimentary Sequence. *Sedimentary Geology*, 148(1/2): 79–103. [https://doi.org/10.1016/s0037-0738\(01\)00211-1](https://doi.org/10.1016/s0037-0738(01)00211-1)
- Han, C., Tian, J. Z., Zhao, R., et al., 2015. Reservoir Space Types and Its Genesis in Tight Calcilutite Rudstone Reservoir of the Lower Part of Member 3 of Shahejie Formation, Shulu Sag. *Acta Petrolei Sinica*, 36(B11): 31–39 (in Chinese with English Abstract)
- Hargrave, J. E., Hicks, M. K., Scholz, C. A., 2014. Lacustrine Carbonates from Lake Turkana, Kenya: A Depositional Model of Carbonates in an Extensional Basin. *Journal of Sedimentary Research*, 84(3): 224–237. <https://doi.org/10.2110/jsr.2014.22>
- Hilfinger, M. F. IV, Mullins, H. T., Burnett, A., et al., 2001. A 2 500 year Sediment Record from Fayetteville Green Lake, New York: Evidence for Anthropogenic Impacts and Historic Isotope Shift. *Journal of Paleolimnology*, 26(3): 293–305. <https://doi.org/10.1023/A:1017560300681>
- Hodell, D. A., Schelske, C. L., Fahnenstiel, G. L., et al., 1998. Biologically Induced Calcite and Its Isotopic Composition in Lake Ontario. *Limnology and Oceanography*, 43(2): 187–199. <https://doi.org/10.4319/lo.1998.43.2.0187>
- Huang, C. Y., Zhang, J. C., Wang, H., et al., 2015. Lacustrine Shale Deposition and Variable Tectonic Accommodation in the Rift Basins of the Bohai Bay Basin in Eastern China. *Journal of Earth Science*, 26(5): 700–711. <https://doi.org/10.1007/s12583-015-0602-3>
- Jarvie, D. M., 2012a. Shale Resource Systems for Oil and Gas: Part 1—Shale-Gas Resource Systems. In: Breyer, J. A., ed., *Shale Reservoirs—Giant Resources for the 21st Century*. *AAPG Memoir*, 97: 69–87. <https://doi.org/10.1306/13321446M973489>
- Jarvie, D. M., 2012b. Shale Resource Systems for Oil and Gas: Part 2—Shale-Oil Resource Systems. In: Breyer, J. A., ed., *Shale Reservoirs—Giant Resources for the 21st Century*. *AAPG Memoir*, 97: 89–119
- Jiang, Z. X., Chen, D. Z., Qiu, L. W., et al., 2007. Source-Controlled Carbonates in a Small Eocene Half-Graben Lake Basin (Shulu Sag) in Central Hebei Province, North China. *Sedimentology*, 54(2): 265–292. <https://doi.org/10.1111/j.1365-3091.2006.00834.x>
- Jiang, Z. X., Li, Q., 2013. Reservoir Characteristics and Evaluation Methods of Tight Lacustrine Carbonates: Example from Shulu Sag in Bohai Bay, China. Unconventional Resources Technology Conference, Denver, USA
- Jiang, Z. X., Liang, C., Wu, J., et al., 2013. Several Issues in Sedimentological Studies on Hydrocarbon-Bearing Fine-Grained Sedimentary Rocks. *Acta Petrolei Sinica*, 34(6): 1031–1039 (in Chinese with English Abstract)
- Jiang, Z. X., Zhang, W., Liang, C., et al., 2014. Characteristics and Evaluation Elements of Shale Oil Reservoir. *Acta Petrolei Sinica*, 35(1): 184–196 (in Chinese with English Abstract)
- Jin, Z., Zhou, Y., Zhang, X., 2002. Lacustrine Carbonate Sedimentary Facies of the Shahejie Formation of Paleogene in Huanghua Depression. *Journal of Paleolimnology*, 4(3): 11–18 (in Chinese with English Abstract)
- Jones, B. F., Bowser, C. J., 1978. The Mineralogy and Related Chemistry of Lake Sediments. In: Baccini, P., ed., *Lakes: Chemistry, Geology, Physics*. Springer, New York. 179–235
- Kelts, K., Hsü, K., 1978. Freshwater Carbonate Sedimentation. In: Baccini, P., ed., *Lakes: Chemistry, Geology, Physics*. Springer, New York. 295–323
- Kelts, K., Talbot, M., 1990. Lacustrine Carbonates as Geochemical Archives of Environmental Change and Biotic/Abiotic Interactions. In: Tilzer, M. M., Serruya, C., eds. *Large Lakes: Ecological Structure and Function*. Springer, Berlin. 288–315. [https://doi.org/10.1007/978-3-642-84077-7\\_15](https://doi.org/10.1007/978-3-642-84077-7_15)
- Kong, X. X., Jiang, Z. X., Han, C., et al., 2016. Laminations Characteristics and Reservoir Significance of Fine-Grained Carbonate in the Lower 3rd Member of Shahejie Formation of Shulu Sag. *Petroleum Geology and Recovery Efficiency*, 23(4): 19–26 (in Chinese with English Abstract)
- Lambert, A., Hsü, K. J., 1979a. Non-Annual Cycles of Varve-Like Sedimentation in Walensee, Switzerland. *Sedimentology*, 26(3): 453–461. <https://doi.org/10.1111/j.1365-3091.1979.tb00920.x>
- Lambert, A., Hsü, K., 1979b. Varve-Like Sediments of the Walensee. In: Schluchter, C., ed., *Moraines and Varves*. Balkema, Rotterdam. 295–302
- Lazar, O. R., Bohacs, K. M., Macquaker, J. H. S., et al., 2015. Capturing Key Attributes of Fine-Grained Sedimentary Rocks in Outcrops, Cores, and Thin Sections: Nomenclature and Description Guidelines. *Journal of Sedimentary Research*, 85(3): 230–246. <https://doi.org/10.2110/jsr.2015.11>
- Lee, C., McKenzie, J. A., Sturm, Z. M., 1987. Carbon Isotope Fractionation and Changes in the Flux and Composition of Particulate Matter Resulting from Biological Activity during a Sediment Trap Experiment in Lake Greifen, Switzerland. *Limnology and Oceanography*, 32(1): 83–96. <https://doi.org/10.4319/lo.1987.32.1.0083>
- Leng, M. J., Marshall, J. D., 2004. Palaeoclimate Interpretation of Stable Isotope Data from Lake Sediment Archives. *Quaternary Science Reviews*,

- 23(7/8): 811–831. <https://doi.org/10.1016/j.quascirev.2003.06.012>
- Lincoln, F., Pratson, J. I., 2000. Abstract: Debris Flows Versus Turbidity Currents: A Modeling Comparison of Their Dynamics and Deposits. *AAPG Bulletin*, 84(2000): 57–72. <https://doi.org/10.1306/a9672b86-1738-11d7-8645000102c1865d>
- Loucks, R. G., Reed, R. M., Ruppel, S. C., et al., 2009. Morphology, Genesis, and Distribution of Nanometer-Scale Pores in Siliceous Mudstones of the Mississippian Barnett Shale. *Journal of Sedimentary Research*, 79(12): 848–861. <https://doi.org/10.2110/jsr.2009.092>
- Loucks, R. G., Reed, R. M., Ruppel, S. C., et al., 2012. Spectrum of Pore Types and Networks in Mudrocks and a Descriptive Classification for Matrix-Related Mudrock Pores. *AAPG Bulletin*, 96(6): 1071–1098. <https://doi.org/10.1306/08171111061>
- Lu, J. M., Ruppel, S. C., Rowe, H. D., 2015. Organic Matter Pores and Oil Generation in the Tuscaloosa Marine Shale. *AAPG Bulletin*, 99(2): 333–357. <https://doi.org/10.1306/08201414055>
- Macquaker, J. H. S., Taylor, K. G., Gawthorpe, R. L., 2007. High-Resolution Facies Analyses of Mudstones: Implications for Paleoenvironmental and Sequence Stratigraphic Interpretations of Offshore Ancient Mud-Dominated Successions. *Journal of Sedimentary Research*, 77(4): 324–339. <https://doi.org/10.2110/jsr.2007.029>
- Mcpherson, J. G., Shanmugam, G., Moiola, R. J., 1987. Fan-Deltas and Braid Deltas: Varieties of Coarse-Grained Deltas. *Geological Society of America Bulletin*, 99(3): 331. [https://doi.org/10.1130/0016-7606\(1987\)99<331:fabdvo>2.0.co;2](https://doi.org/10.1130/0016-7606(1987)99<331:fabdvo>2.0.co;2)
- Milliken, K. L., Rudnicki, M., Awwiller, D. N., et al., 2013. Organic Matter-Hosted Pore System, Marcellus Formation (Devonian), Pennsylvania. *AAPG Bulletin*, 97(2): 177–200. <https://doi.org/10.1306/07231212048>
- Milliken, K., 2014. A Compositional Classification for Grain Assemblages in Fine-Grained Sediments and Sedimentary Rocks. *Journal of Sedimentary Research*, 84(12): 1185–1199. <https://doi.org/10.2110/jsr.2014.92>
- Morellón, M., Valero-Garcés, B., Anselmetti, F., et al., 2009. Late Quaternary Deposition and Facies Model for Karstic Lake Estanya (North-Eastern Spain). *Sedimentology*, 56(5): 1505–1534. <https://doi.org/10.1111/j.1365-3091.2008.01044.x>
- Mulder, T., Syvitski, J. P. M., Migeon, S., et al., 2003. Marine Hyperpycnal Flows: Initiation, Behavior and Related Deposits: A Review. *Marine and Petroleum Geology*, 20(6/7/8): 861–882. <https://doi.org/10.1016/j.marpetgeo.2003.01.003>
- Mulder, T., Zaragosi, S., Razin, P., et al., 2009. A New Conceptual Model for the Deposition Process of Homogenite: Application to a Cretaceous Megaturbidite of the Western Pyrenees (Basque Region, SW France). *Sedimentary Geology*, 222(3/4): 263–273. <https://doi.org/10.1016/j.sedgeo.2009.09.013>
- Mullins, H. T., 1998. Environmental Change Controls of Lacustrine Carbonate, Cayuga Lake, New York. *Geology*, 26(5): 443. [https://doi.org/10.1130/0091-7613\(1998\)026<0443:eccolc>2.3.co;2](https://doi.org/10.1130/0091-7613(1998)026<0443:eccolc>2.3.co;2)
- Myrow, P. M., Hiscott, R. N., 1991. Shallow-Water Gravity-Flow Deposits, Chapel Island Formation, Southeast Newfoundland, Canada. *Sedimentology*, 38(5): 935–959. <https://doi.org/10.1111/j.1365-3091.1991.tb01880.x>
- Osleger, D. A., Heyvaert, A. C., Stoner, J. S., et al., 2009. Lacustrine Turbidites as Indicators of Holocene Storminess and Climate: Lake Tahoe, California and Nevada. *Journal of Paleolimnology*, 42(1): 103–122. <https://doi.org/10.1007/s10933-008-9265-8>
- Pacton, M., Fiet, N., Gorin, G. E., 2007. Bacterial Activity and Preservation of Sedimentary Organic Matter: The Role of Exopolymeric Substances. *Geomicrobiology Journal*, 24(7/8): 571–581. <https://doi.org/10.1080/01490450701672042>
- Platt, N. H., 1989. Lacustrine Carbonates and Pedogenesis: Sedimentology and Origin of Palustrine Deposits from the Early Cretaceous Rupelo Formation, W Cameros Basin, N Spain. *Sedimentology*, 36(4): 665–684. <https://doi.org/10.1111/j.1365-3091.1989.tb02092.x>
- Platt, N., Wright, V. P., 1991. Lacustrine Carbonates: Facies Models, Facies Distributions and Hydrocarbon Aspects. In: Anadón, P., Cabrera, Li., Kelts, K., eds., Lacustrine Facies Analysis. John Wiley & Sons, New York. 57–74
- Pu, X. G., Zhou, L. H., Xiao, D. Q., et al., 2011. Lacustrine Carbonates in the Southwest Margin of the Qikou Sag, Huanghua Depression, Bohai Bay Basin. *Petroleum Exploration and Development*, 38(2): 136–144. [https://doi.org/10.1016/s1876-3804\(11\)60022-0](https://doi.org/10.1016/s1876-3804(11)60022-0)
- Qiu, L. W., Jiang, Z. X., Liang, H. B., 2010. Lime Mudstone—A Kind of Carbonate Rock of Terrigenous Mechanical Origin. *Journal of China University of Petroleum*, 34(6): 1–7 (in Chinese with English Abstract)
- Ramos-Guerrero, E., Berrio, I., Fornós, J., et al., 2000. The Middle Miocene Son Verdera Lacustrine-Palustrine System (Santa Margalida Basin, Mallorca). *AAPG Studies in Geology*, 46: 441–448
- Ren, Y. Q., 1986. Depositional Environments of Shulu Depression-Viewed from the Point of Micropaleobotanic Florae. *Acta Sedimentologica Sinica*, 4(4): 101–108 (in Chinese with English Abstract)
- Romero-Viana, L., Julià, R., Camacho, A., et al., 2008. Climate Signal in Varve Thickness: Lake la Cruz (Spain), a Case Study. *Journal of Paleolimnology*, 40(2): 703–714. <https://doi.org/10.1007/s10933-008-9194-6>
- Schieber, J., Southard, J. B., Schimmelmann, A., 2010. Lenticular Shale Fabrics Resulting from Intermittent Erosion of Water-Rich Muds—Interpreting the Rock Record in the Light of Recent Flume Experiments. *Journal of Sedimentary Research*, 80(1): 119–128. <https://doi.org/10.2110/jsr.2010.005>
- Soreghan, M. J., 1998. Facies Distributions within an Ancient Asymmetric Lake Basin: The Apache Canyon Formation, Bisbee Basin, Arizona. In: Pitman, J. K., Carroll, A. R., eds., Modern and Ancient Lake Systems. Utah Geological Association Guidebook 26. C & M Press, Denver. 163–190
- Stabel, H., 1985. Mechanisms Controlling the Sedimentation Sequence of Various Elements in Prealpine Lakes. In: Stumm, W., ed., Chemical Processes in Lakes. John Wiley and Sons, New York. 143–167
- Stanley, D. J., 1981. Unifites: Structureless Muds of Gravity-Flow Origin in Mediterranean Basins. *Geo-Marine Letters*, 1(2): 77–83. <https://doi.org/10.1007/bf02463322>
- Stow, D. A. V., Bowen, A. J., 1978. Origin of Lamination in Deep Sea, Fine-Grained Sediments. *Nature*, 274(5669): 324–328. <https://doi.org/10.1038/274324a0>
- Stow, D. A. V., Shanmugam, G., 1980. Sequence of Structures in Fine-Grained Turbidites: Comparison of Recent Deep-Sea and Ancient Flysch Sediments. *Sedimentary Geology*, 25(1/2): 23–42. [https://doi.org/10.1016/0037-0738\(80\)90052-4](https://doi.org/10.1016/0037-0738(80)90052-4)
- Sturm, M., Matter, A., 1978. Turbidites and Varves in Lake Brienz (Switzerland): Deposition of Clastic Detritus by Density Currents. In: Matte, A., Tucker, M. E., Modern and Ancient Lake Sediments. *International Association of Sedimentologists Special Publication*, 2: 147–168. <https://doi.org/10.1002/9781444303698.ch8>
- Sumner, E. J., Talling, P. J., Amy, L. A., 2009. Deposits of Flows Transitional between Turbidity Current and Debris Flow. *Geology*, 37(11): 991–994. <https://doi.org/10.1130/g30059a.1>
- Talling, P. J., Masson, D. G., Sumner, E. J., et al., 2012. Subaqueous Sediment

- Density Flows: Depositional Processes and Deposit Types. *Sedimentology*, 59(7): 1937–2003. <https://doi.org/10.1111/j.1365-3091.2012.01353.x>
- Taylor, K. G., Macquaker, J. H. S., 2000. Early Diagenetic Pyrite Morphology in a Mudstone-Dominated Succession: The Lower Jurassic Cleveland Ironstone Formation, Eastern England. *Sedimentary Geology*, 131(1/2): 77–86. [https://doi.org/10.1016/s0037-0738\(00\)00002-6](https://doi.org/10.1016/s0037-0738(00)00002-6)
- Teranes, J. L., McKenzie, J. A., Bernasconi, S. M., et al., 1999. A Study of Oxygen Isotopic Fractionation during Bio-Induced Calcite Precipitation in Eutrophic Baldeggersee, Switzerland. *Geochimica et Cosmochimica Acta*, 63(13/14): 1981–1989. [https://doi.org/10.1016/s0016-7037\(99\)00049-6](https://doi.org/10.1016/s0016-7037(99)00049-6)
- Tripsanas, E. K., Bryant, W. R., Phaneuf, B. A., 2004. Depositional Processes of Uniform Mud Deposits (Unifites), Hedberg Basin, Northwest Gulf of Mexico: New Perspectives. *AAPG Bulletin*, 88(6): 825–840. <https://doi.org/10.1306/01260403104>
- Tucker, M. E., Wright, V. P., 1990. Carbonate Sedimentology. Wiley-Blackwell, London
- Valero-Garcés, B., Morellón, M., Moreno, A., et al., 2014. Lacustrine Carbonates of Iberian Karst Lakes: Sources, Processes and Depositional Environments. *Sedimentary Geology*, 299(2): 1–29. <https://doi.org/10.1016/j.sedgeo.2013.10.007>
- Wang, D., Feng, X., 2002. Research on Carbon and Oxygen Geochemistry of Lower Paleozoic in North China. *Acta Geologica Sinica—Chinese Edition*, 76(3): 400–408 (in Chinese with English Abstract)
- Wang, G. L., Wang, T. G., Simoneit, B. R. T., et al., 2010. Sulfur Rich Petroleum Derived from Lacustrine Carbonate Source Rocks in Bohai Bay Basin, East China. *Organic Geochemistry*, 41(4): 340–354. <https://doi.org/10.1016/j.orggeochem.2009.12.010>
- Wilkin, R. T., Barnes, H. L., Brantley, S. L., 1996. The Size Distribution of Framboidal Pyrite in Modern Sediments: An Indicator of Redox Conditions. *Geochimica et Cosmochimica Acta*, 60(20): 3897–3912. [https://doi.org/10.1016/0016-7037\(96\)00209-8](https://doi.org/10.1016/0016-7037(96)00209-8)
- Zha, X. P., Zhao, Y. Y., Zheng, Y. F., 2010. An Online Method Combining a Gasbench II with Continuous Flow Isotope Ratio Mass Spectrometry to Determine the Content and Isotopic Compositions of Minor Amounts of Carbonate in Silicate Rocks. *Rapid Communications in Mass Spectrometry*, 24(15): 2217–2226. <https://doi.org/10.1002/rcm.4632>
- Zhang, J. G., Jiang, Z. X., Jiang, X. L., et al., 2016. Oil Generation Induces Sparry Calcite Formation in Lacustrine Mudrock, Eocene of East China. *Marine and Petroleum Geology*, 71(3): 344–359. <https://doi.org/10.1016/j.marpetgeo.2016.01.007>
- Zhang, W. C., Cui, Z. Q., Han, C. Y., et al., 2001. Basin Evolution during Palaeogene and Petroleum Potentials of Central Hebei (Jizhong) Depression. *Journal of Paleolimnology*, 3(1): 45–54 (in Chinese with English Abstract)
- Zhang, X. W., Scholz, C. A., 2015. Turbidite Systems of Lacustrine Rift Basins: Examples from the Lake Kivu and Lake Albert Rifts, East Africa. *Sedimentary Geology*, 325(6): 177–191. <https://doi.org/10.1016/j.sedgeo.2015.06.003>
- Zhao, X. Z., Jiang, Z. X., Zhang, R. F., et al., 2015. Geological Characteristics and Exploration Practices of Special-Lithology Tight Oil Reservoirs in Continental Rift Basins: A Case Study of Tight Oil in Shahejie Formation, Shulu Sag. *Acta Petrolei Sinica*, 36(B11): 1–9 (in Chinese with English Abstract)
- Zhao, X. Z., Li, Q., Jiang, Z. X., et al., 2014. Organic Geochemistry and Reservoir Characterization of the Organic Matter-Rich Calcilutite in the Shulu Sag, Bohai Bay Basin, North China. *Marine and Petroleum Geology*, 51(2): 239–255. <https://doi.org/10.1016/j.marpetgeo.2013.12.014>
- Zheng, L. J., Jiang, Z. X., Liu, H., et al., 2015. Core Evidence of Paleoseismic Events in Paleogene Deposits of the Shulu Sag in the Bohai Bay Basin, East China, and Their Petroleum Geologic Significance. *Sedimentary Geology*, 328: 33–54. <https://doi.org/10.1016/j.sedgeo.2015.07.013>
- Zolitschka, B., 2007. Varved Lake Sediments. In: Saraswat, R., Nigam, R., eds., *Encyclopedia of Quaternary Science*. Elsevier, Amsterdam. 3105–3114
- Zolitschka, B., Francus, P., Ojala, A. E. K., et al., 2015. Varves in Lake Sediments—A Review. *Quaternary Science Reviews*, 117(6): 1–41. <https://doi.org/10.1016/j.quascirev.2015.03.019>